universität wien

MASTERARBEIT / MASTER'S THESIS

Titel der Maserarbeit / Title of the Master's Thesis

„ Optimised micropatterning workflows for positioning of migratory cell lines on EM substrates "

verfasst von / submitted by

Maximilian Schuster BSc

Angestrebter akademischer Grad / in partial fulfilment of the requirements for the degree of

Master of Science (MSc)

Wien, 2023 / Vienna, 2023

Studienkennzahl lt. Studienblatt / degree programme code as it appears on the student record sheet:	UA 066 830
Studienrichtung lt. Studienblatt / degree programme as it appears on the student record sheet:	Masterstudium Molecular Microbiology, Microbial Ecology and Immunobiology
Betreut von / Supervisor:	Assistant Professor Mag. Dr. Florian Schur

1 Contents

2 Zusammenfassung

Kryo-Elektronentomographie (ET) ermöglicht die Visualisierung von 3D-Strukturen von Objekten im nativen, hydrierten Zustand. Zur Durchführung von kryo-ET an Säugetierzellen werden diese auf Elektronenmikroskopie (EM)-Gittern angezüchtet, überzogen mit einer Kohlenstoffschicht. Allerdings neigen die Zellen dazu, sich zufällig zu verteilen und sich in der Nähe oder auf dem Gitternetzwerk anzuhaften, da durch dieses eine höhere Stabilität des Substrats gegeben ist. Für die ET-Aufnahme ist es jedoch unerlässlich, dass sich die Zellen im Zentrum eines einzelnen Gitterquadrats in unmittelbarer Nähe zum Zentrum des Gitters befinden. Maskenloses Photodrucken ist eine Technik zur Kontrolle der Zellausrichtung durch Mikromuster von extrazellulären Matrixproteinen auf empfindlichen EM-Gittern. In dieser Studie wurde ein Protokoll zur effizienten Mikromusterung mit dem PRIMO-Gerät entwickelt, wobei darauf geachtet wurde, die benötigte Vorbereitungszeit, teure Reagenzien und das Bewegen der Gitter mit Pinzetten zu minimieren. Verschiedene Säugetierzelltypen wurden getestet und der Erfolgsgrad der mikromusterten Gitter wurde bewertet. Die Ergebnisse zeigten eine 3-5-fache Steigerung der korrekt positionierten Zellen für nachfolgende kryo-ET-Arbeitsabläufe. Die Technik zum Säen der Zellen wurden an die spezifischen Anforderungen der verschiedenen Zelltypen angepasst. Die Verwendung von 3D-gedruckten EM-Gitterhaltern für den Musterdruckprozess wurde ebenfalls bewertet, erwies sich jedoch in deren aktueller Qualität als ungeeignet. Das Verhalten verschiedener Zelltypen auf verschiedenen Musterformen wurde bewertet, was das Potenzial mikrogemusterter Gitter zur Kontrolle der morphologischen Eigenschaften von Säugetierzellen verdeutlichte. Insgesamt präsentiert diese Arbeit ein optimiertes Mikromusterungsprotokoll mit signifikanten Verbesserungen bei der Zellpositionierung für kryo-ET-Studien.

3 Abstract

Cryo-electron tomography (ET) enables the visualization of 3D structures of objects in their native hydrated state. To perform cryo-ET on mammalian cells, they are seeded on carbon-coated electron microscopy (EM) grids. However, the cells tend to spread randomly and adhere near or on the mesh of the grid, as higher stability of the substrate is given. For ET acquisition, it is essential that the cells are located in the centre of an individual grid square, in close proximity to the centre of the grid. Maskless photopatterning is a technique used to control cell orientation by micropatterning extracellular matrix proteins on delicate EM grids. This study aimed to develop a protocol for efficient micropatterning with the PRIMO device, minimizing the required preparation time, expensive reagents, and grid handling. Various mammalian cell types were tested, and the success rate of micropatterned grids was evaluated. The results showed a 3-5x increase in properly positioned cells for subsequent cryo-ET workflows. Seeding procedures were adapted to meet the specific requirements of different cell types. The use of 3D printed EM grid holders for the patterning workflow was also assessed but found unsuitable in their current quality. The behaviour of different cell types on various pattern shapes was evaluated, demonstrating the potential of micropatterned grids to control mammalian cell morphology. Overall, this work presents a streamlined micropatterning protocol with significant improvements in cell positioning for cryo-ET studies.

4 Introduction

4.1 The principle of electron microscopic applications and their requirements

Since the mid of the last century, electron microscopy (EM) has been an essential tool to study the ultrastructural features of diverse structures in a broad variety of sample types [1], [2]. The principle of this microscopic technique is to direct an electron beam of several hundred kilovolts with electron lenses towards a specimen placed on the microscopic stage, and create an image using an electron detector [3]. For all transmission electron microscopy (TEM) based applications, the specimen has to be stable in the vacuum within the microscope [1]. Further, the thickness of the specimen is critical, as the electron beam has to pass through the object and the resolution of the acquired image decreases with higher sample thickness [2]. Higher electron voltage in general allows the imaging of thicker samples and increases the resolution of the EM image. Nevertheless, specimens dedicated for EM acquisition are in general very sensitive, higher electron dosages can easily ionize the sample, creating free radicals by breaking atomic bonds [4]. The sample further can heat up when exposed to high electron dosages, leading to shifts during acquisition or destruction of the object of interest [1], [4]. Developments in technical terms increased the potential of EM applications tremendously and is ongoing since. This is true regarding the electromagnetic coils leading the electrons or the stabilization of the specimen with different microscopic stages [2]. Especially the development of cameras and detectors to detect the incoming electrons [2], as well as the introduction of novel image processing and analysis tools [5] enhanced the possibilities to apply EM in the scientific field.

In the early 1980's, cryo-EM was introduced into the scientific field, a technique used to acquire EM images of a specimen frozen at cryogenic temperatures, to conserve a structure of interest in its native state in vitreous ice [6]. Specimens, positioned on an EM sample carrier, can be plunge-frozen by rapid freezing at temperatures below -190 °C [7], for example by submersion in liquid ethane. Further progress was made by the introduction of high-pressure freezing [8], overcoming the limitation of ice-crystal damage and insufficient freezing of thicker samples [9]. The frozen sample subsequently has to be lifted out of the carrier used for freezing, to be positioned on the EM sample carrier for further processing and imaging.

Electron tomography (ET) was introduced in 1968 [10] and until the 1990's, with the automatization of several steps, further adapted for biological research [11]. By using an electron microscope stage capable of tilting the sample, it became possible to capture a series of two-dimensional images of the same object from different registered angles with TEM [12]. Subsequently, the three-dimensional structure of the object can be reconstructed from the individual projections, and the object is displayed as three-dimensional volume (the electron tomogram) [10]. Cryo-electron tomograms usually have a resolution in the nanometre range, limited by several factors, including: i) the pixel size of the camera chip, ii) the missing wedge in tomographic data, which refers to the angular range where imaging is not possible due to stage tilting limitations [2], [11], iii) the defocus during acquisition and iv) the thickness of the specimen [4]. Without applied thinning processes, bulkier samples and thicker regions of single cells are not suitable by default for cryo-ET. Only the peripheries of most samples can be observed with cryo-ET. In the case of single cells, this mainly refers to the lamellipodia and filopodia. Lamellipodia are thin extensions of the plasma membrane of a cell [13]. They are essential for cell adherence to the substrate via integrins expressed on the surface and for cell migration [13]. Filopodia are thin plasma-membrane protrusions, extending from the leading edge of a lamellipodium [14]. They are involved in sensing the extracellular environment, signal transport as well as cell migration [14].

Focused ion beam (FIB) milling was first introduced in 1975 [15] and later on developed to cryo-FIB milling for frozen samples [16], [17] to overcome some limitations of cryo-ET. Only

shortly after, the technique was presented as strategy to reduce the thickness of frozen cellular samples in dedicated areas to be analysed with cryo-TEM techniques [18]. Essential to make FIB-milling applicable for frozen samples is the fact, that during the thinning process the sample is not warmed up to cause devitrification [16]. This is true for any cryo-EM technique. In general, an ion beam typically originating from a gallium source is used to produce a lamella from a bulky sample, by stepwise removal of matter layer by layer. Scanning electron microscopy (SEM) is used to observe the process of sample milling with minimal sample damage due to irradiation (FIB-SEM) [16], [19]. The technique is used on bulky specimens and specimen areas by default not suitable for EM applications. Necessary for the processing is knowledge about the spatial and axial position of the structures of interest.

A sample for TEM or ET is in general placed on a carrier specifically designed for TEM applications, known as EM grids. These grids can be made out of copper, gold, titanium or molybdenum, the material depends on the specific application. For seeding of living cells, grids made out of biocompatible materials are required [20]. An individual EM grid is about 30 µm thin and consists of a ring with 3 mm diameter, inside the ring grid bars span across the opening to support the placed sample [20]. The grid bars are usually orientated in a 90° angle to form squares of a certain size; the thickness of the bars and the size of the squares is indicated with the mesh-size of a grid. To further support the sample placed on the EM grid, it can be coated with different films like Formvar, holey carbon (HC), continuous carbon (CC) or lacey carbon film [2]. Those options come with different film thickness and, in case of the HC film, with different size of the holes, to keep the thickness of the observed object plus the film as low as possible to maximize the image resolution. The choice of a certain type of grid and the coating is depending on the sample to be observed with TEM, the structure of interest, the type of electron microscope and further factors. For certain sample processing and imaging applications, only defined areas on EM grids are applicable. For ET, the specimen has to be located in close proximity to the centre of the grid to enable the image acquisition of the tilted object (indicated in Figure 1A) [20]. The grid squares around the centre are in general useable for acquisition of electron tomograms, as it is possible to perform the tilt series and record the series of EM images in registered angles from usually +60° to -60° [20]. Further, to avoid impaired view by the grid bars, the sample has to be placed in the centre of an individual grid square [20]. As for cryo-FIB milling, in general every position on an EM grid can be thinned, but a close proximity to the grid bars makes it more difficult and takes more time. Therefore, the centre of an individual grid square is preferred, also for eventual improvements like semi-/automated FIB milling.

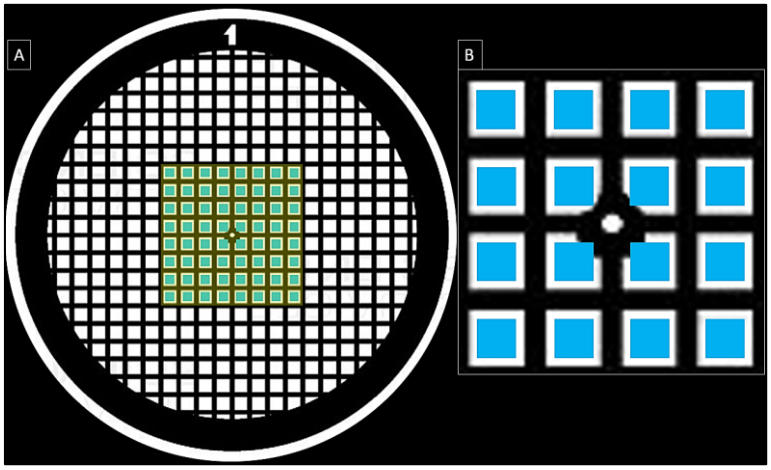

Figure 1: A 200 mesh EM grid, with regions for ET marked: ***A)*** *View of a whole grid; the central 8x8-grid squares marked with a transparent yellow square are considered applicable for cryo-ET, as a tilt required to acquire the individual images is possible. The region in each grid square applicable for ET is marked with a blue square.* ***B)*** *A closeup on the central 4x4 grid-squares, showing the areas in each grid-square in more detail.*

4.2 Difficulties with EM-based applications

The difficulties with eukaryotic cells come with the culturing of the specimen directly on the carbon-coated EM grids for subsequent EM imaging [1]. In general, the supporting carbon film on the EM grid is first coated with a layer of molecules to enable adherence of the specimen to the surface. These molecules can be different proteins present in the extracellular matrix (ECM proteins), produced by diverse cell types in a multicellular organism or in cell culture [21]. A different adhesive molecule is for example poly-L-lysine (PLL). Multi-adhesive ECM proteins used for the purpose of promoting adhesion on EM grids include, among others, fibrinogen, fibronectin, collagen and laminin [22], [23]. The strategy to coat the whole grid with the molecules is necessary to ensure adhesion of the specimen to the carbon surface, but enables the cells to adhere, spread and migrate uncontrolled, though not randomly. Cells prefer to stay close or on the grid bars, as higher stability of the substrate is given compared to the centre of the grid squares [24]. As stated before, this behaviour is opposing the conditions necessary for ET acquisition, and is an issue scientist tried to resolve over the last decades.

In general, two fundamentally different approaches were developed since the early 1990's to engineer the microenvironment of living samples and spatially control the adhesion of cells. The first strategy is the construction of a molecular pattern by transferring the molecules sequentially to the location of interest, and was in literature termed constructive or additive patterning [25]–[28]. Applications working like this include dip-pen nanolithography, polymer-pen lithography and soft lithography. These methods have the shortcomings, that highly controlled environments and low temperatures are required, the approaches are very slow, indirect and they cannot be scaled without effort, but enable printing of molecules with nanometre resolution [26]. The second strategy to spatially control the transfer of adhesive molecules onto a designated surface is termed destructive or subtractive patterning [26], [27]. Techniques using this strategy include nanografting, nanoshaving, anodic oxidation and millipede [26], as well as techniques like photo patterning and laser patterning of proteins [29], [30]. In general, these techniques describe the coating of the surface by a layer inhibiting the adherence of the protein of choice, and destruction of this layer by exposure to high energy in designated areas [26]. Subsequently, the desired molecule is added, only able to adhere in the areas where the inhibiting layer was depleted [26], [27], [30]. Photo patterning in the traditional sense relies on the use of a photomask to block the light and induce destruction of the surface coating only on designated areas. [29] While this strategy is relatively fast in depletion, it relies on the prior production of the photomask and alignment of it on the surface to be patterned on [29]. Laser patterning on the other hand does not require a photomask, but as a point source of light is used to deplete the surface coating, the writing process of the pattern takes significantly longer [29], [30]. These shortcomings were resolved, when in 2016 light induced molecular adsorption of proteins (LIMAP) was published [27].

4.2.1 LIMAP & PRIMO

LIMAP is a photo patterning technique, where a water-soluble photo initiator is used to deplete an antifouling (AF) layer when activated by UV light. The principle of this patterning technique was further adapted by the use of digital micromirror devices (DMD) in widefield microscopic systems for easier and high-throughput printing of proteins [27]. This makes the use of a physical photomask during light projection obsolete, as the DMD is able to control the areas of projected light in micrometre resolution, depending on the DMDs properties and the optical system used for projection. In 2016, Alvèole introduced the PRIMO photo patterning system, a DMD device equipped with a 375 nm UV laser light source [27], and recently the PRIMO 2 with a 365 nm LED light source. This device is able to project the UV light with a resolution of up to 1.2 µm. With this application it became possible to project a prior drawn digital photomask [27]. This digital mask can be easily exchanged and adapted. By sequential projection of

different patterns and protein incubation, it is possible to perform multi-protein patterning and it is also possible to pattern in gradients by projecting light with different light powers or exposure times [27]. The general workflow for the application of the PRIMO device for micropatterning of proteins is shown in Figure 2. Due to its broad and easy application, LIMAP has been surging over the last few years in the biological field and diverse applications had been published since. The PRIMO photo patterning system is not only used for micropatterning of proteins on diverse substrates [31], [32], but also for the structuration of hydrogels [33] or the microfabrication of UV sensitive resists like SU-8 [34].

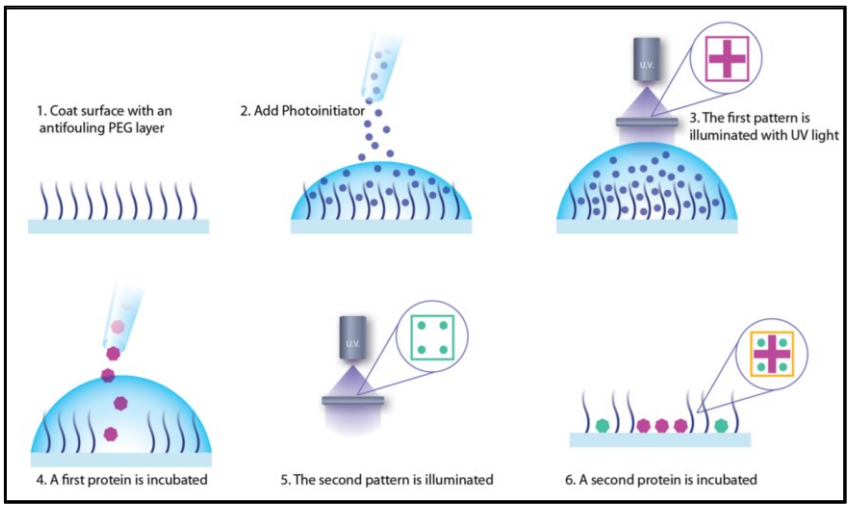

Figure 2: Principal workflow for LIMAP: The different sample carrier preparation steps are shown. ***1)*** *A surface is coated with an AF layer.* ***2)*** *The photo initiator is added.* ***3)*** *A pattern is projected with an optical system with UV light.* ***4)*** *A molecule is incubated on the surface, able to adhere only on the patterned areas.* ***5)*** *Optional: A second pattern is projected on the same surface.* ***6)*** *A different molecule is incubated. The optional workflow leads to multi-molecule patterns. Figure adapted from Strale et al. (2016)* [27].

In more detail, to perform LIMAP, the first step is to coat a surface with a molecule like poly-L-lysine (PLL), laminin or (3-Aminopropyl) triethoxysilane (APTES). The next step is the grafting of those molecules with an AF agent like poly-ethylene glycol (PEG), a polymer of ethylene oxide, in the form of methoxy-poly-ethylene glycol-succinimidyl valerate (mPEG-SVA, shown in Figure 3 A) [27]. The photo chemical reaction is performed by an UV-sensitive initiator like 4-benzoylbenzyl-trimethylammonium chloride, commonly known as PLPP (shown in Figure 3 B) [35]. The principle of the photo scission reaction under the influence of high-energy yielding light and oxygen is displayed in Figure 3 C.

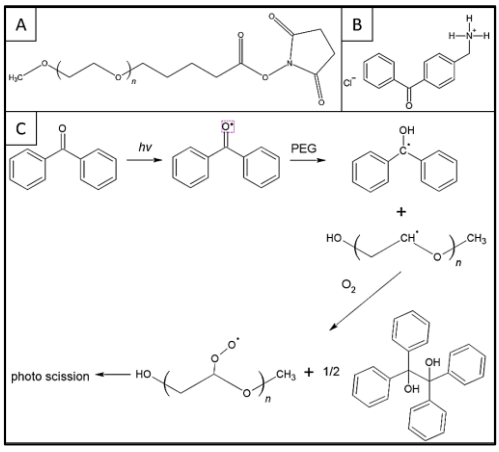

Figure 3: LIMAPs photo scission reaction, substrate and photo initiator: ***A)*** *The structure formular of the AF agent mPEG-SVA.* ***B)*** *The structure formular of the PLPP photo initiator.* ***C)*** *The photo scission reaction of the PLPP photo initiator shown on the PEG-chain under the influence of UV (*hv*) and oxygen. The scission event takes place at a random location in the chain. Created with ChemSketch* [36]

The AF PEG coating is important for two reasons in regard of micropatterning on surfaces to be applied for single cell organisms: first, during the process of patterning, it restricts the adhesion of the incubated proteins from the non-depleted areas [27]. Second, when the cells are seeded on the processed sample carrier, it confines the cells to the patterned areas due to its AF properties [37]. In general, any protein can be incubated on the photo patterned sample carrier, rendering these areas adhesive for the specimen seeded on it and inducing specific behaviour. For cellular specimens, the ECM proteins fibronectin, fibrinogen or laminin are commonly applied in diverse protocols [20], [24], [31], [32], [38], [39].

4.2.2 ECM proteins commonly used for coating sample carriers and their purpose in nature

ECM glycoproteins mediate connections in the ECM between different ECM components, and between the matrix and soluble compounds in the extracellular environment. Further and most importantly for the purpose to serve in EM-based experiments, they serve as link between cells and their substrate. In cell culture this refers to the sample carrier like a glass surface or the carbon film on an EM grid. Two glycoproteins often used for functionalizing sample carrier surfaces are fibronectin and laminin. [21], [40]

4.2.2.1 Fibronectin, its roles in vivo and its effect on cells in culture

Fibronectin is an adhesive extracellular glycoprotein, able to establish cell-ECM links between diverse integrins on the cellular surface to different molecules in the ECM like collagen, heparin and fibrin [21]. Several isoforms of fibronectin exist, depending on their type they are able to bind different ligands and integrins [40]. All isoforms originate from a single fibronectin gene, spliced in alternative ways [40]. They are able to transmit mechanical signals from cell to cell and make the cell sensitive and responsive to their environment [40]. They mediate processes like embryogenesis and wound healing when acting in concert with other compounds of the ECM and molecules on the cell surface [41]. When used for cells in culture, e.g., for diverse fibroblast cells, they mediate among others cell attachment, migration, adhesion and spreading [41]. The general structure and the sites of the diverse interacting molecules of a fibronectin dimer is shown in Figure 4.

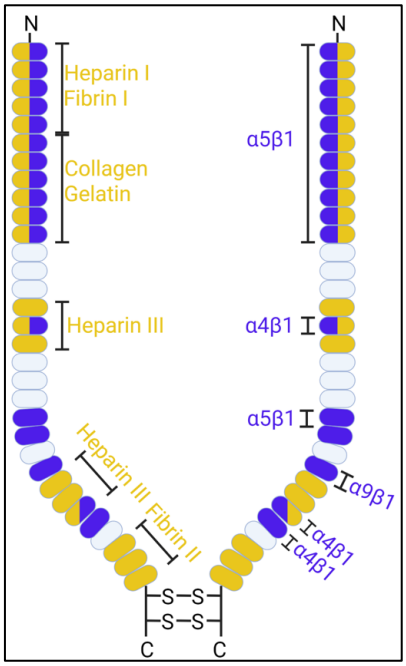

Figure 4: The general structure of a fibronectin dimer: The two fibronectin molecules are connected via disulphide bonds at the C-terminal ends. Each of the individual fibronectin chains contains sequences to bind to diverse integrins on cell surfaces (visualized in blue) and binding sites different ECM components (shown in yellow). Created with BioRender [42]*, information about binding sites from Dalton and Lemmon (2021)* [40].

4.2.2.2 Laminin, its roles in vivo and its effect on cells in culture

Laminin is a heterotrimeric glycoprotein composed of three polypeptides (α, β and γ), which can vary between different laminin types. In multicellular organisms, laminins are exclusively restricted to the basement membranes [40]. They contain interaction domains connecting to diverse ECM components and to cell membrane receptors [21]. Laminins are one of the key components of the basal lamina and is the primary organizer of the lamina, together with different collagen types, nidogen and perlecan [22], [43]. The connection to cells is mediated via various integrins on the cell surface and the α-chain of the laminin trimer. Depending on the type of α-chain, different integrins are interacting and leading to a number of possible cellular behaviours, including cell adhesion, migration, differentiation, proliferation, polarity and apoptosis [43]. In cell culture, the effect of laminin adhered to the surface of the sample carrier therefor depends on the type of laminin and the type of cell used for the experiment, but in general lead to cell adhesion, the formation of lamellipodia, cell migration and proliferation. Figure 5 shows the general structure of the laminin heterotrimer, as well as possible interaction partners in the ECM and on the cell surface.

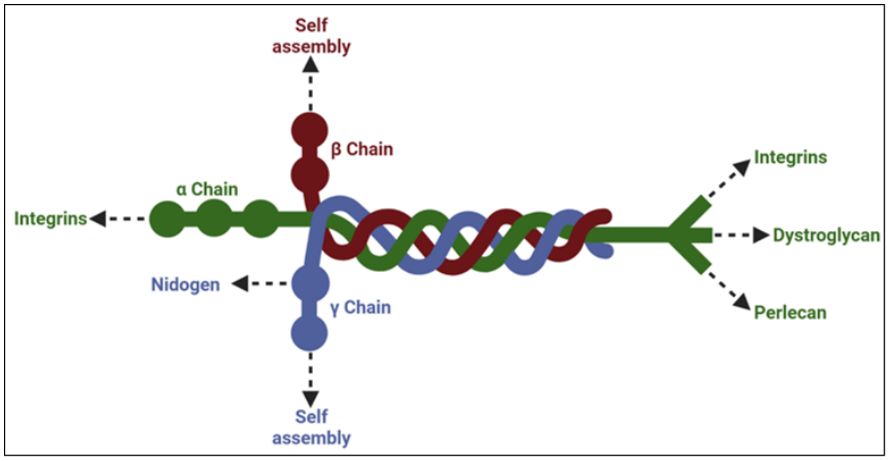

Figure 5: The general structure of laminins: The three chains α, β and γ are shown after assembling into the laminin heterotrimer. On the respective domains, the different interaction partners are indicated, including different ECM components, other laminin molecules for self-assembly and integrins on cell membranes. Created with BioRender [42]*, Information about binding sites and inspiration about design from Alberts et al. (2015)* [44].

4.3 Cells investigated in this project

4.3.1 HeLa cells

HeLa cells are a well-known line of human cancer cells that have been widely used in scientific research for 70 years since their collection from a biopsy of a cervical cancer from Henrietta Lacks [45]. They were the first human cells to be successfully grown in a laboratory and have since become an invaluable resource for biomedical studies. HeLa cells have contributed to numerous advancements in areas such as vaccine development, virology, cell biology, genetics, cancer research, drug discovery, gene mapping, and assisted reproductive technologies [46]–[48]. Their robustness and ability to be propagated indefinitely have made them a vital tool in understanding human biology and developing medical treatments. HeLa cells typically exhibit an adherent, epithelial-like morphology characterized by a flattened and elongated shape with a prominent nucleus and distinct cell boundaries [49]. HeLa cells are not a migrating cell line, their broad application in the scientific field and for different micropatterning experiments makes them an ideal candidate to evaluate the general functionality of new developed protocols for sample carrier preparation.

4.3.2 B16-F1 melanoma cells

A melanoma is the most aggressive form of skin cancer, these cells have a high metastatic potential and can spread fast from their origin to distant organs [50]. B16-F1 melanoma cells

are a commonly studied migrating cell line, derived from a melanoma tumour in a C57BL/6 mouse [51]. They exhibit characteristics of malignant melanoma, including uncontrolled proliferation and invasive behaviour [51]. B16-F1 cells grown in cell culture conditions and adhered to a surface show spindle-like morphological features, but also epithelial cell-like filopodia [52]. They are widely used in research to study melanoma progression, metastasis, and evaluate potential therapies [50], [53].

4.3.3 Rat2 fibroblast cells

Fibroblasts typically have an elongated, spindle-shaped morphology with a flattened nucleus and abundant cytoplasmic extensions called filopodia [54]. They represent a migrating, predominant stomal cell type, present in soft connective tissues [54]. Rat1 cells are a fibroblast cell line derived from rat connective tissue that are commonly used in scientific research [55]. They are derived from embryonic rat fibroblasts and serve as a model system to study various biological processes [55]. Rat2 cells are one of the sublines originating from the Rat1 cells, they are cultivated in laboratories to investigate cellular behaviour and response to experimental conditions or stimuli [55]. Rat2 fibroblast cells play a crucial role in understanding the structure of the cytoskeleton, cell signalling, gene expression, cell cycle regulation, and cell migration, among others [56]–[59]. These cells are valuable tools for researchers studying fundamental cellular processes and testing the effects of drugs or substances on cell growth and behaviour [58]–[60].

4.4 Aims & Objectives of the thesis project

The project had the aim to optimize the LIMAP technique, to functionalize sample carriers applicable for cryo-ET in a fast and easy way, with little hand-on time and grid handling in general, to reduce the loss of expensive materials and the time spent for carrier preparation. The focus of this project lied on the overall cellular morphology and behaviour (attachment, migration and proliferation) of adherent mammalian cell lines, namely for HeLa cells, wildtype B16-F1 melanoma cell and Rat2 fibroblast cells as a proof of principle. Three objectives were worked on:

4.4.1 The establishment of LIMAP and its application on EM-grids

Following the guidelines for the patterning of EM grids with the PRIMO 2® system (Avèole Lab) [61], as well as protocols for micropatterning published by Toro-Nahuelpan [62] and recently by Engel and colleagues [32], [39], the general concept of micropatterning on EM grids was tested and the workflow optimized. To ease the delicate handling of the fragile grids, grid holders [63] were used for the steps involving cell culture, and their compatibility with the LIMAP technique was evaluated.

4.4.2 Optimization of cell seeding on grids for high-throughput cryo-ET workflows

The second objective was integrating the photo patterned EM grids into an established workflow for downstream cryo-ET experiments and to ultimately reduce time spent on screening EM grids for individual cells. Laminin was used for protein patterning for the three cell types and its potential to induce cell adhesion in designated places was evaluated. With an increasing number of well-positioned cells per grid, the use of materials can be reduced, as well as the number of cells required for seeding. Precise control over the spatial orientation also has the potential to help overcoming limitations in the downstream sample preparation processes. An increased number of well-positioned cells per grid further offers the possibility to automate the tomographic image acquisition. By using micropatterned EM grids, individual cells can be optimally and reproducibly positioned to be accessible for milling with cryo-FIB after vitrification. This offers the opportunity to semi-/automated the thinning process, without the need of constant supervision. Streamlining this step in the preparation procedure for in-cell structural studies is critical to establish high-throughput cryo-ET pipelines.

4.4.3 Control of cell behaviour and morphology with different pattern shapes

Different pattern shapes were designed according to the general guidelines from Alvèole [64]. The effect of the different protein pattern shapes was evaluated for the three cell types in regard of their behaviour, namely their migration, spreading and their proliferation on the grids. Different cell behaviour can serve to investigate different experimental goals. The results of this objective were used to give an idea on how different pattern shapes can be used to reach condition in a reliable and reproductive manner. Further, a timepoint for each cell line was evaluated to perform fixation and stop the cell cycle, before cells duplicate and individual grid squares are occupied by multiple cells.

5 Materials and Methods

5.1 Cell Culture

Wildtype B16-F1 melanoma cells and HeLa cells were cultured in Dulbecco's modified Eagle's medium (DMEM GlutaMAX™, ThermoFischer Scientific, #31966047), supplemented with 10% (v/v) fetal bovine serum (ThermoFischer Scientific, #10270106) and 1% (v/v) penicillin-streptomycin (ThermoFischer Scientific, #15070063). Rat2 fibroblast cells were cultured in Dulbecco's modified Eagle's medium (DMEM GlutaMAX™, ThermoFischer Scientific, #31966047), supplemented with 10% (v/v) fetal bovine serum (ThermoFischer Scientific, #10270106), 1% (v/v) penicillin-streptomycin (ThermoFischer Scientific, #15070063) and 1% non-essential amino acids (MEM NEAA (100x), Gibco, #11140050). Cells were incubated in tissue-culture treated culture dishes (Corning, #CLS430166) at 37°C and 5% CO_2.

Cells were split every 48 hours, the cell cultures were first inspected via a benchtop widefield microscope (Olympus CKX41, equipped with a 10x/ NA 0.25 CAchN PhP objective (Olympus N5229200) and a UI-3480LE-M-GL monochrome camera (IDS)) in transmitted light with phase contrast, to confirm overall viability of the cells and absence of bacterial or fungal infection. In a cell culture laminar flow, the culture medium was then removed with a vacuum pump. The culture was washed with 4 ml Phosphate Buffered Saline (PBS pH 7.2 (1x), gibco, REF# 20012-019) which was removed again with the vacuum pump. 0.4 ml trypsin**,** warmed up to 37 °C in a water bath, was added at a concentration of 0.05% (gibco, REF# 25300-054) for B16-F1 melanoma cells and HeLa cells and 0.25% (gibco, REF# 25200-056) for Rat2 fibroblasts to the culture dish stored in the incubator, until the cells detached from the dish surface. Subsequently, 4 ml of cell culture medium, warmed up to 37 °C in a water bath, was added to the dish; the culture medium for B16-F1 melanoma cells and HeLa cells contained 10% (v/v) fetal bovine serum to inactivate the trypsin, the medium for Rat2 fibroblasts did not contain the fetal bovine serum, to avoid the fast reattachment of the Rat2 cells to the culture dish before cells were prepared for seeding on EM grids (see section "Cell Seeding" below). Depending on the growth rate of the different cell types, the cell lines were split at different ratios, at a confluency of about 90%: B16-F1 melanoma cells were split in a ratio of 1/20, HeLa cells in a ratio of 1/10 and Rat2 fibroblast cells in a ratio of 1/20. In the new cell culture dish for Rat2 fibroblasts, cell culture medium, warmed up to 37 °C in a water bath, containing 10% (v/v) was used to inactivate the trypsin and enable attachment of the cells.

5.2 Photo patterning on glass bottom dishes: test general functionality of the AF layer, the PRIMO principle & cell behaviour

A 35 mm glass bottom dish (Thermo Scientific™, CAT# 150680) was passivated by the same strategy used later on for the EM grids. The glass surface was rendered hydrophilic using a plasma cleaner (HARRICK PLASMA, PDC-001) at medium RF power (20 W) settings for 2 minutes, and then incubated for 30 minutes with poly-L-lysine (PLL, Sigma-Aldrich, CAS# 25988-63-0, P4707) at room temperature (RT). The grids were washed 3x with 0.1 M, pH 8.4 HEPES (N-2-Hydroxyethylpiperazine-N'-2-ethane sulphonic acid, ROTH, CAS# 7365-45-9)

without drying, by removing most of the liquid from the grids, adding HEPES and waiting about 30 seconds before the liquid was removed again and fresh one added. Following, the glass was incubated with 0.1 g/ml poly-ethylene glycol-succinimidyl valeric acid (mPEG-SVA, MW 5.000, Laysan Bio Inc) in HEPES (0.1 M, pH 8.4) for 1 hour at RT. The grids were washed 3x with Milli-Q water (MQ) without drying. After the last washing step, the excess liquid was removed and the glass surface dried at RT before used for micropatterning.

After fully dried, the glass bottom dish was coated with an UV sensitive photo initiator (PLPP gel, Alvèole, Paris, France), diluted 1:3 with 70% Ethanol (EtOH). After the gel dried on the surface, the dish was placed on the microscopic stage of an inverted Ti2-E (Nikon), equipped with the Alvéole Primo 2 photopatterning system (Alvéole, Paris, France), 2 filter wheels containing a Di03-R405-t1 dichroic mirror (Semrock), a Plan Fluor air objective 10x/ NA 0.3 DIC1 N1 (Nikon, MRH00101) for photo patterning glass surfaces, a Ti2-S-SE-E motorized stage (Nikon), the Perfect Focus System 4 (Nikon) and a Moment CMOS 12-bit camera (Teledyne). 50% of the glass bottom were exposed to the 365 nm UV light by placing full DMD fields over one half of the glass surface, to deplete the AF layer by using 30 mJ/mm^2 exposure with 100% light power. FIJI was used as platform for the µManager software equipped with the Leonardo plugin (Alvéole, Paris, France) to control the Primo device and project the patterns from a 365 nm, 4.0 mW LED light source.

Following the photo patterning, the PLPP gel was dissolved by applying MQ to the glass bottom dish, which was exchanged three times. The AF (AF) layer was rehydrated by adding PBS. Following, Laminin (Sigma-Aldrich, CAS# 114956-81-9, L2020) in a 25-50 µg/ml concentration in laminin coating buffer (50 mM tris and 150 mM NaCl, pH 7.4) was incubated for one hour in the glass bottom dish. Next, the ECM protein solution was washed 3x with laminin coating buffer, exchanged for cell culture medium for HeLa cells (DMEM (GlutaMAX™, ThermoFischer Scientific, #31966047), supplemented with 10% (v/v) fetal bovine serum (ThermoFischer Scientific, #10270106) and 1% (v/v) penicillin-streptomycin (ThermoFischer Scientific, #15070063)), and stored in the incubator.

Finally, the dish was stored at 37 °C in the cell culture incubator, and 10 µl of cell dilution from a HeLa cell culture in a 4 cm cell culture dish at 100% confluency was seeded into the glass bottom dish. The dish was then put on the stage of an inverted Ti2-E widefield microscope (Nikon), equipped with a Plan Fluor air objective 10x/ NA 0.3 DIC1 N1 (Nikon, MRH00101), a DIC slider (Nikon) adjusted to 45°, a Ti2-S-SE-E motorized stage (Nikon), the Perfect Focus System 3 (Nikon) and a DS-Qi2 monochrome camera (Nikon). To enhance the contrast of the transmitted light images, differential interference contrast (DIC) was used for acquisition. To keep the seeded cells in optimal culture conditions, the microscope was equipped with an incubation box connected to a heating unit keeping the temperature inside at 37 °C, and a gas incubation system (ibidi, Gas Incubation System for CO2 – Blue Line, CAT# 11920) to keep the atmosphere at 80% humidity and 5% CO_2 during the whole image acquisition. To observe cell adhesion and migration a timelapse over 2 hours with 5 minutes interval was performed. The cell behaviour of HeLa cells on the side with depleted AF layer was compared to the side with functional AF layer.

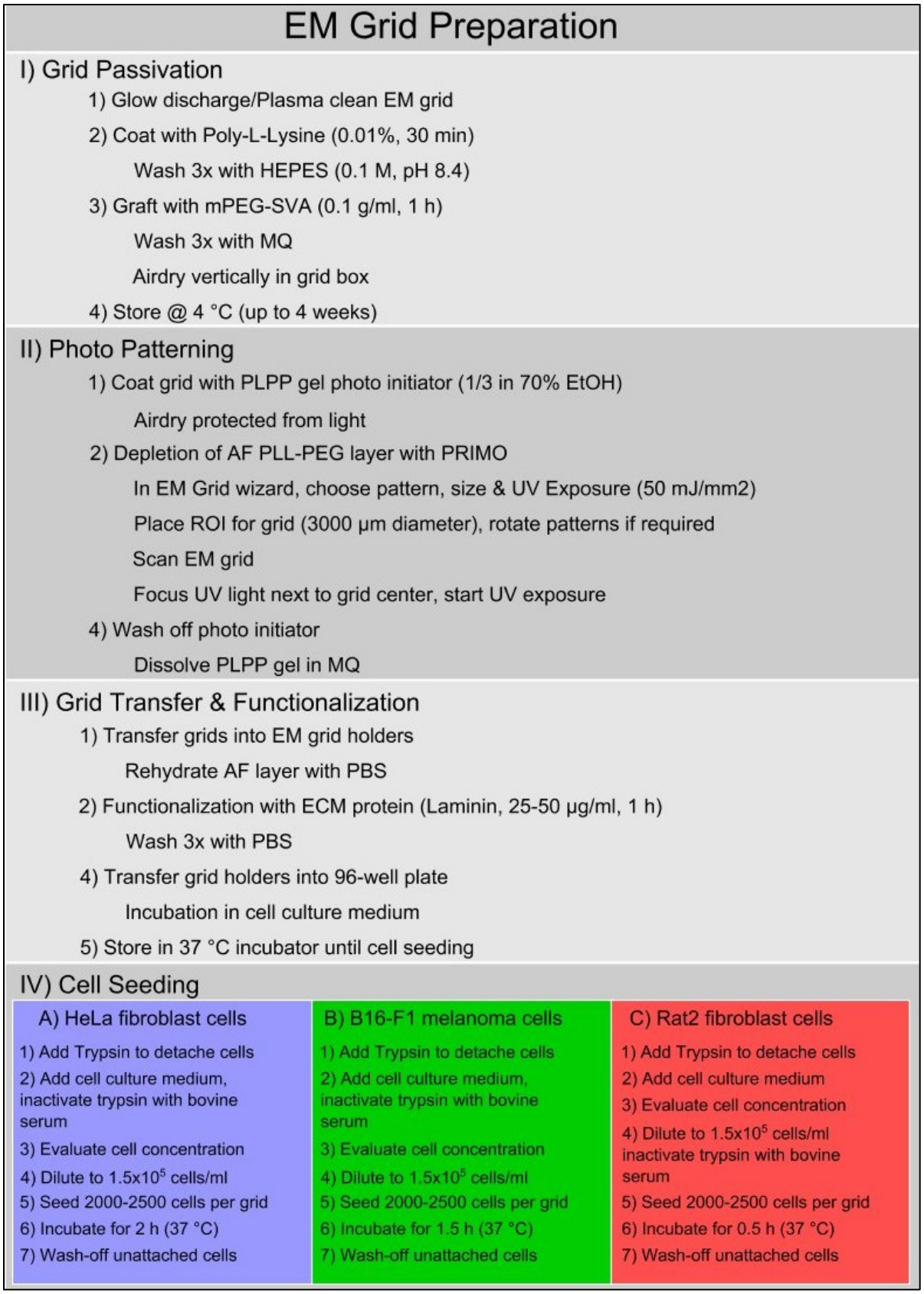

Figure 6: The whole workflow of the protocol for EM grids developed during the project, summing up the individual steps to coat an EM grid with an AF PLL-PEG layer (I), depleting it in designated area using the PLPP gel photo initiator and the PRIMO 2 micropatterning system (II), functionalize the designated areas with the ECM protein laminin (III) and seeding different cell types onto the processed grid (IV). The whole protocol is described in all detail on the following pages.

5.3 EM Grid Preparation and Handling

5.3.1 Grid Passivation

1) Plasma Cleaning: The grids were placed carbon-film up on a microscopic glass slide, covered with PARAFILM® M (Sigma-Aldrich, # BR701501) and plasma cleaned for 2 min in a plasma cleaner (HARRICK PLASMA, PDC-001) at medium RF power (20 W). Alternatively, an ELMO glow discharge system (Cordouan technologies) was used to render the EM grids hydrophilic. The effect of both machines on the resulting pattern and AF quality was evaluated by performing the whole photo patterning protocol described here, including seeding B16-F1 melanoma cells and observation of cell attachment to the patterned areas.

2) Coating with PLL: A 2-step procedure was applied for passivation of the EM grids without moving them from the glass slide: first, the plasma cleaned grids were incubated for 30 min in a 0.01% PLL solution (Sigma-Aldrich, CAS# 25988-63-0, P4707) at RT. The grids were washed 3x with HEPES 0.1 M, pH 8.4 (N-2-Hydroxyethylpiperazine-N'-2-ethane sulphonic acid, ROTH, CAS# 7365-45-9) without drying, by removing most of the liquid from the grids, adding HEPES and waiting about 30 seconds before the liquid was removed again and fresh one added.

3) Grafting with mPEG-SVA: Subsequently, most of the washing solution was removed from the grids and 0.1 g/ml poly-ethylene glycol-succinimidyl valeric acid (mPEG-SVA, MW 5.000, Laysan Bio Inc) in HEPES (0.1 M, pH 8.4) was added, to be incubated at RT for 1 h. The mPEG-SVA powder was previously weighted to 14 mg in Eppendorf tubes, the aliquots stored at -20 °C and warmed up to room temperature before dissolving in HEPES. The solution was prepared directly before use, as the half-life time of mPEG-SVA in solution is about 10 min [39]. 140 µl 0.1 M HEPES, pH 8.4 was added to reach the aimed 0.1 g/ml and mixed by pipetting until the liquid turned from opaque to clear, the resulting volume is enough to cover at least 10 grids with a bubble of mPEG-SVA solution. The grids were washed 3x with MQ without drying, by removing most of the liquid from the grids, adding MQ and waiting about 30 seconds before the liquid was removed again and fresh one added.

4) Storage: The grids were carefully removed from the last washing solution with tweezers, the excess liquid removed with a sheet of Whatman paper (Sigma-Aldrich, WHA2105841) from the side without carbon coating. The grids stored vertically in a grid box, to avoid tearing of the delicate carbon film during drying on a surface. The grids were stored at 4 °C and were used for micropatterning up to 4 weeks after passivation.

5.3.2 Photo patterning

1) Coating with photo initiator: The dry grids, coated with the passivating PLL-PEG layer, were placed carbon film up on a #1.5 glass cover slip (VWR, #48393-241). A 1:3 solution of UV sensitive photo initiator (PLPP gel, Alvèole, Paris, France) was prepared in 70% EtOH, a droplet of 3 µl was added on each grid, while gently pinning the grid to the glass surface with the tweezers to avoid adhesion of the grid to the droplet on the pipette tip. After 15 min at RT, the PLPP gel solution was dry and ready for patterning. At all steps when PLPP photo initiator was involved, ambient light was excluded as much as possible by keeping the grids in a dark environment to reduce unwanted activation of the PLPP gel and uncontrolled digestion of the AF layer.

2) Depletion of the AF layer with PRIMO: The coverslip was placed on the stage of an inverted Ti2-E widefield microscope (Nikon), equipped with the Alvéole Primo 2 photopatterning system (Alvéole, Paris, France), 2 filter wheels containing a Di03-R405-t1 dichroic mirror (Semrock), a CFI Super Plan-Fluor ELWD objective 20xC/NA 0.45 (Nikon, MRH08230) for photopatterning on EM grids, a Ti2-S-SE-E motorized stage (Nikon), the Perfect Focus System 4 (Nikon) and a Moment CMOS 12-bit camera (Teledyne). The digital masks for photopatterning were drawn

using Inkscape (Figure 7 A) according to the protocol to create patterns for photo patterning provided by Alvèole ([64]). FIJI was used as platform for the µManager software equipped with the Leonardo plugin (Alvéole, Paris, France) to control the Primo device and project the patterns from a 365 nm, 3.1 mW LED light source.

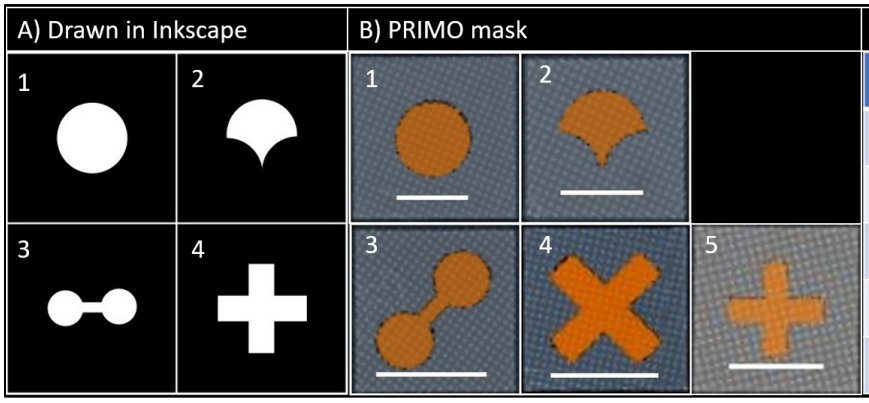

Pattern Shape	Area [µm²]
Circle	1257
Fan	753
Dumbbell (45°)	992
Cross (45°)	1474
Cross (40 µm)	455

Figure 7: Patterns: ***A)*** *The 4 patterns drawn with Inkscape according to the protocol provided by Alvèole and to be included in the Leonardo EM grid wizard and projected on EM grid squares: Circle-, Fan-, Dumbbell- and Cross-Pattern.* ***B)*** *The 4 patterns as photomask displayed in the EM grid wizard, on 200 mesh HC gold grids. The dumbbell- and cross-patterns were rotated by 45° in the Leonardo EM grid wizard, to increase the patterned area. To compare, the unrotated cross pattern is shown in Image B5. The scale bars in B1, B2 and B5 are 40 µm, the scale bars in B3 and B4 are 50 µm.* ***C)*** *For the 5 photomasks, the areas were calculated.*

The wizard for EM grid photopatterning with automated grid scanning and grid-square detection was used to place the individual patterns in the centre of each grid square. The field of view was moved to the centre of the grid and a square in the very centre was used to adjust the focus of a small circle projected manually with the PRIMO 2, the light emitted by the activated photo initiator was clearly visible. In the EM grid wizard of the Leonardo software, the following parameters were adjusted: i) UV dose, ii) pattern size, iii) the rotation of the patterns, iv) the light power. The patterns were projected through the holey-carbon film with a 50 mJ/mm² dosage with 100% light power. The size and rotation of the patterns depended on the shape of the pattern and are shown in Figure 7 B. The rotation function was used to fit the Cross and Dumbbell pattern with maximal area available for cell adhesion on the individual grid squares, by rotating 45° relative to the grid bars. For comparison, the cross pattern is shown in not rotated in Image B5. For the Circle pattern, the rotation was not required. The fan pattern was rotated to define the orientation of the tip end and the opposing rounded edge. For all patterns, the area was measured using FIJI and listed in Figure 7 C.

4) Wash off photo initiator: Following the micropatterning, the PLPP gel photo initiator was dissolved in a droplet of MQ, the liquid was exchanged 2x without drying to ensure complete removal of the PLPP gel. The grids were stored up to 24 hours vertically in a grid box at 4 °C, before the grids were patterned with ECM protein.

5.3.3 Protein functionalization

1) Transfer grids into EM grid holders: To transfer the grids without breaking the fragile carbon layer, the whole cover slip was inserted into a bubble of MQ. The grids were carefully moved towards the edge of the cover slip and picked up with tweezers when overhanging on the edge of the cover slip. The bubble of MQ is required as the grids can barely be picked up directly from the flat glass surface, and need to stay hydrated. The grids were placed in 3D-printed grid holders [63], placed on a microscopic slide covered with Parafilm. To ease the insertion of the grids into the grid holders, a droplet of PBS was placed beforehand on the grid holders, and the grid were inserted into that droplet at a 45° angle. The AF PLL-PEG brush was rehydrated with PBS for 10 minutes on the grid surface.

2) Functionalization with ECM protein: The grid was incubated in ECM protein Laminin (Sigma-Aldrich, CAS# 114956-81-9, L2020) for 1 h at room temperature in a 25-50 µg/ml concentration in Laminin (Sigma-Aldrich, CAS# 114956-81-9, L2020) in laminin coating buffer (50 mM tris and 150 mM NaCl, pH 7.4). Following, the grid was washed 3x with the respective ECM protein buffer.

To visualize the different shapes of projected patterns**,** 300 mesh Cu grids with CC film as well as 200 and 150 mesh HC Au grids were incubated in a solution of fluorescently labelled fibrinogen (Alexa Fluor 488, ThermoFischer Scientific, #F13191) in sodium bicarbonate buffer pH 8.3 (Merck, CAS# 144-55-8) at a concentration of 50 µg/ml for 15 min at room temperature. The impact of different UV exposures was tested by comparing fluorescent signals from grids patterned with 20 and 50 mJ/mm^2. Further, to test the possibility to pattern molecules apart from ECM proteins, 200 mesh R2/2 HC grids were incubated in a solution of fluorescently labelled monoclonal antibody MOPC-173 immunoglobulin (Cy5.5, BioLegend®, # 400257) in 0.09% sodium azide pH 7.2 at a concentration of 0.2 mg/mL for 5 min at room temperature.

3) Transfer into 96-well plates and incubation in cell culture medium: The grid holders with the grids were then transferred into 96 well-plates (Merck, Z707902) after excessive buffer solution was removed. To each grid-holder, 70 µl of cell-culture medium (Dulbecco's modified Eagle's medium (DMEM GlutaMAX™, ThermoFischer Scientific, #31966047), supplemented with 10% (v/v) fetal bovine serum (ThermoFischer Scientific, #10270106) and 1% (v/v) penicillin-streptomycin (ThermoFischer Scientific, #15070063)) was added. The medium for Rat2 fibroblasts additionally contained 1% (v/v) non-essential amino acids (MEM NEAA (100x), Gibco, #11140050).

4) Storage: The wells were checked with the cell culture microscope, to confirm that the grids are actually sitting in the grid holders and not on the edges, to avoid excessive tilt of the grid. The 96-well plate was than stored in an incubator at 37 °C until cells were seeded on the grids.

5.4 Cell Seeding

B16-F1 melanoma cells, HeLa cells and Rat2 fibroblasts were split as stated above. The cells in the dish with 90% confluency were used for seeding on the EM grids prepared with passivation, photopatterning and protein functionalization. Three biological replicates were done with each three technical replicates, including each time one grid for negative and one grid for second control. As negative control, grids not subjected to the passivation and photopatterning protocol but only the functionalization with ECM proteins were used, to investigate behaviour of the cells under standard experimental conditions without photopatterning procedures. As a second control, grids subjected to passivation and functionalization, but not photopatterning were used, to assess the functionality of the AF PLL-PEG layer.

1) Cell count: First, an aliquot of 200 µl of cell dilution was taken from the cell culture dish and put in a 1.5 ml Eppendorf tube. 10 µl of this cell dilution was used to perform cell counting, by mixing with 10 µl Trypan Blue solution (0.4% liquid, Sigma-Aldrich, CAS# 72-57-1) and pipetting into a chamber of a counting slide (Dual Chamber for Cell Counter, BIO-RAD, Cat# 145-0011). The slide was injected into an automated cell counter (TC20™ Automated Cell Counter, BIO-RAD) to evaluate the total amount of cells per ml, living cells per ml and the ratio of both. The total amount of living cells per ml was used to calculate the required ratio of a dilution containing 1.5 x 10^5 cells per ml.

2) Cell dilution: Subsequently, a volume required to produce a cell dilution of 150 µl, with 1.5 x 10^5 cells per ml was transferred from the original 200 µl and diluted with cell culture medium, warmed up to 37 °C in a water bath. In the case of Rat2 fibroblasts, the fresh medium for

dilution now also contained 10% (v/v) fetal bovine solution, to deactivate the trypsin present in the medium.

3) Cell seeding: Next, the 96-well plate containing the grid holders loaded with EM grids was taken out of the incubator and transferred into the laminar flow. To seed 2000 cells per grid, 13.3 µl of the cell dilution with 1.5 x 10^5 cells/ml was taken up in a 200 µl pipette tip, slowly moved into the well plate until the tip touches the cell culture medium. With a slow and steady movement, the cell dilution was pipetted into the medium to avoid movement of the grid in the grid holders, and to ensure that the cells sink onto the grid and not excessively around it into the well of the well plate. The 96-well plate was put into the incubator to enable the cells to sink on the surface on the grid, and attach to the functionalized areas.

5.4.1 Wash-off unattached cells

After some time, the cells sitting on the micropatterns were able to attach to the carbon surface. This time depended on the cell type: for B16-F1 melanoma cells attached during 1.5 hours, HeLa cells in 2 hours and Rat2 fibroblasts already after 20-30 minutes. After this time had passed, the 96-well plate was removed from the incubator, to wash off all cells not adhered to the patterned ECM protein, but positioned on the AF PLL-PEG layer. To do so, 50 µl of fresh, 37 °C warm cell culture medium was pipetted into the wells loaded with grid holders and removed again without moving the pipette tip too close to the grid, to not dislocate the grid from the grid holder. 2-3x pipetting of fresh medium and removal of it was required to remove most of the cells from the AF layer. The grids were observed with the cell culture microscope, to assess the success of the wash-off procedure.

5.5 Observation of cell behaviour

The 96-well plate was then moved from the cell culture room onto the stage of an inverted Ti2-E widefield microscope (Nikon), equipped with a Plan Fluor air objective 10x/ NA 0.3 DIC1 N1 (Nikon, MRH00101), a DIC slider (Nikon) adjusted to 45°, a Ti2-S-SE-E motorized stage (Nikon), the Perfect Focus System 3 (Nikon) and a DS-Qi2 monochrome camera (Nikon). To enhance the contrast of the transmitted light images, differential interference contrast (DIC) was used for acquisition. To keep the seeded cells in optimal culture conditions, the microscope was equipped with an incubation box connected to a heating unit keeping the temperature inside at 37 °C, and a gas incubation system (ibidi, Gas Incubation System for CO2 – Blue Line, CAT# 11920) to keep the atmosphere at 80% humidity and 5% CO_2 during the whole image acquisition. As the grids in the grid holders as well as the holders in the well-plate were able to slightly move due to stage movement between multiple positions, the XY coordinates of each position were adjusted 2 hours after start of the acquisition if needed, and a Z stack of 100 µm range with 20 µm interval was recorded. The imaging was performed overnight for 12 hours after cell seeding, with 10 minutes interval between the time points.

5.6 Image processing and analysis

The multipoint files were split into individual files automatically by the NIS Elements software (Nikon) after the acquisition was finished. All resulting images were further processed using the FIJI. [65] All Z planes out of focus were manually removed. A macro was used to project all remaining Z planes into a 2-dimensional image. PowerPoint was further used to overlay the resulting JGEP image with the image of the photomask from the Leonardo software, to indicate the location and orientation of the protein patterns.

To analyse the results, first the total amount of grid squares fully visible was automatically counted in each image using a FIJI macro, all squares not fully visible because the view was blocked by the grid holder were excluded. This macro converted the input TIFF file to binary to create a mask for subsequent particle analysis. The minimum size of each grid square for 200 mesh gold grids was defined with 6250 µm^2 and a circularity of 0.6-0.95. The number of

counted squares and the mask with the counts were than displayed. Every broken grid square was subtracted from the result.

To evaluate the success of spatially controlled cell positioning using photo patterning, the area of an individual grid square applicable for cryo-EM and FIB-milling was annotated by a mask (see Figure 8). To be counted as applicable for further processing for cryo-ET, a single cell had to be located fully in that area. All squares with more than 2 cells and all squares without cells were counted accordingly. The same procedure was performed for all grids on which the photo patterning protocol was performed and all control grids.

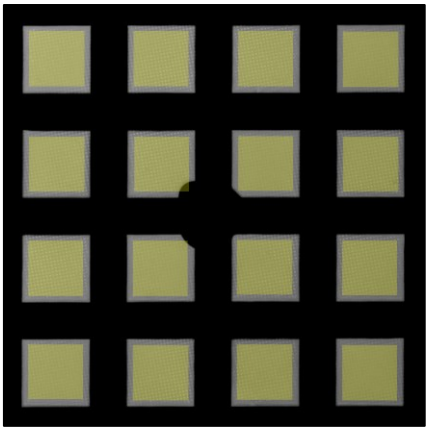

Figure 8: Areas on a grid-square applicable for ET: 4x4-grid square image around the centre of a 200 mesh HC gold EM grid coated with HC film. The yellow squares indicate the areas applicable for processing for subsequent FIB-milling and ET acquisition; only single cells located completely in the yellow squares, without approaching the grid bars, are counted as usefully placed.

6 Results

6.1 Initials experiments to test materials and devices

6.1.1 Test the general functionality of the AF layer

To investigate, if all reagents used for the micropatterning protocol are functional, a 35 mm glass bottom dish was treated with the described protocol for micropatterning. All images in Figure 9 show the same glass bottom dish at different time points. The PRIMO device was used to deplete the AF layer on one half of the glass surface (Figure 9 A), the HeLa cells were able to adhere on the glass surface, spread and migrate. The other half of the glass, not exposed to UV light, was coated an intact AF layer (Figure 9 B). HeLa cells on the AF layer were not able to adhere and spread. This experiment confirmed the functionality of the materials used, as well of the PRIMO photo patterning system applied for this study.

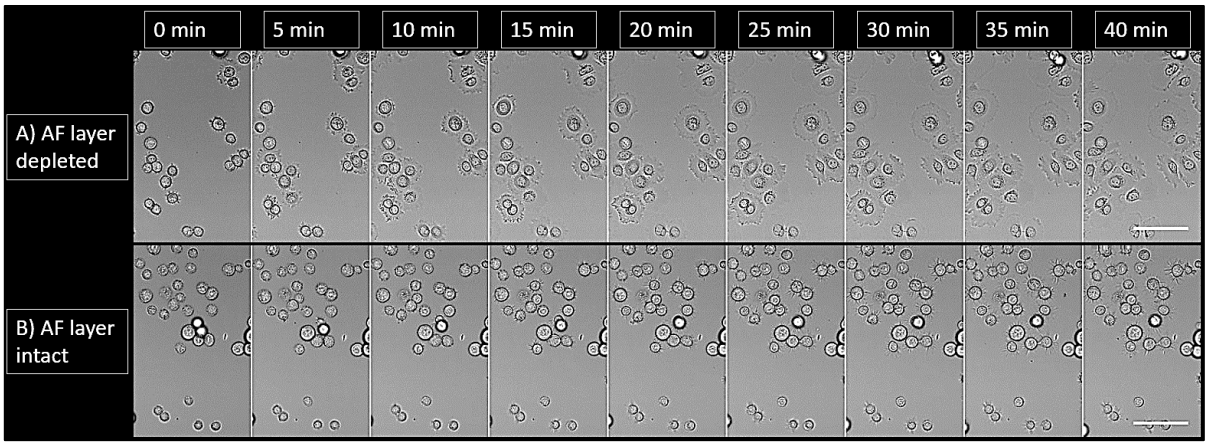

Figure 9: HeLa cells on a glass bottom dish with and without depleted AF layer: The whole glass surface was coated with the PLL-PEG AF layer. ***A)*** *One half of the dish was subjected to the UV light projected by the PRIMO (AF depleted).* ***B)*** *The other half remained untreated (AF layer intact). The timelapse over 40 minutes is shown with a 5-minute interval. HeLa cells were not able to spread on the half intact AF layer, opposingly they were able to spread and migrate on the half of the dish where the AF was depleted by photo initiator activity. Scale bars are 100 µm in size.*

6.1.2 LIMAP on EM grids, confirmed with fluorescent signal on HC as well as CC grids

To test the general functionality of the developed protocol to photo pattern EM grids, fluorescent labelled proteins were used to functionalize the grids. The resulting fluorescent patterns were visualized using fluorescence widefield microscopy. In Figure 10 A and B, the same 200 mesh R2/2 HC grid is shown, before and after incubation of the ECM protein fibrinogen, labelled with Alexa Fluor 488. No AF layer was grafted on this grid, the overall fluorescent signal clearly increases after the protein was incubated. This increase can be seen when comparing the intensity profile along the grey lines, the respective graphs are shown under the images of the grids. In Figure 10 C and D, the same 150 mesh R2/2 HC grid is shown, before and after incubating the fluorescent labelled ECM protein. The grid was coated before imaging with the AF layer, restricting the protein from adhering to the carbon surface. Following, the overall fluorescence on the HC film does not increase, shown in the intensity profiles under the respective images. In Figure 10 E and F, two different 150 mesh R2/2 HC grids are shown. The full protocol for micropatterning was applied to both grids, the grids only differ in the UV exposure used for photo patterning (Figure 10 E: 20 mJ/mm^2; Figure 10 F: 50 mJ/mm^2). On both grids, the fluorescence signal on the AF layer has a similar intensity as the grid with AF layer only (Figure 10D). The fluorescence on the patterned area in Figure 10 E is about 22% higher than the signal from the AF layer. The pattern on the grid in Figure 10 F is roughly 50% higher than the signal from the AF layer, the drops of intensity can be explained by the line for the intensity profile crossing a hole in the carbon film. Figure 10 G shows 3x3 grid-squares of a 300 mesh Cu grid, coated with a CC film. The full patterning protocol was performed on this grid, and Alexa Fluor 488 labelled fibrinogen was used to functionalize the grid. This result confirms, that the developed protocol is applicable to grids coated with different carbon films. Figure 10 H shows 2x2 grid-squares of a 200 mesh R2/2 HC grid. This grid was subjected to the full protocol for photo patterning, but instead of the ECM protein, a secondary antibody labelled with Cy5.5 was used to functionalize the pattern. This result shows the general functionality of the photo patterning technique for different protein types.

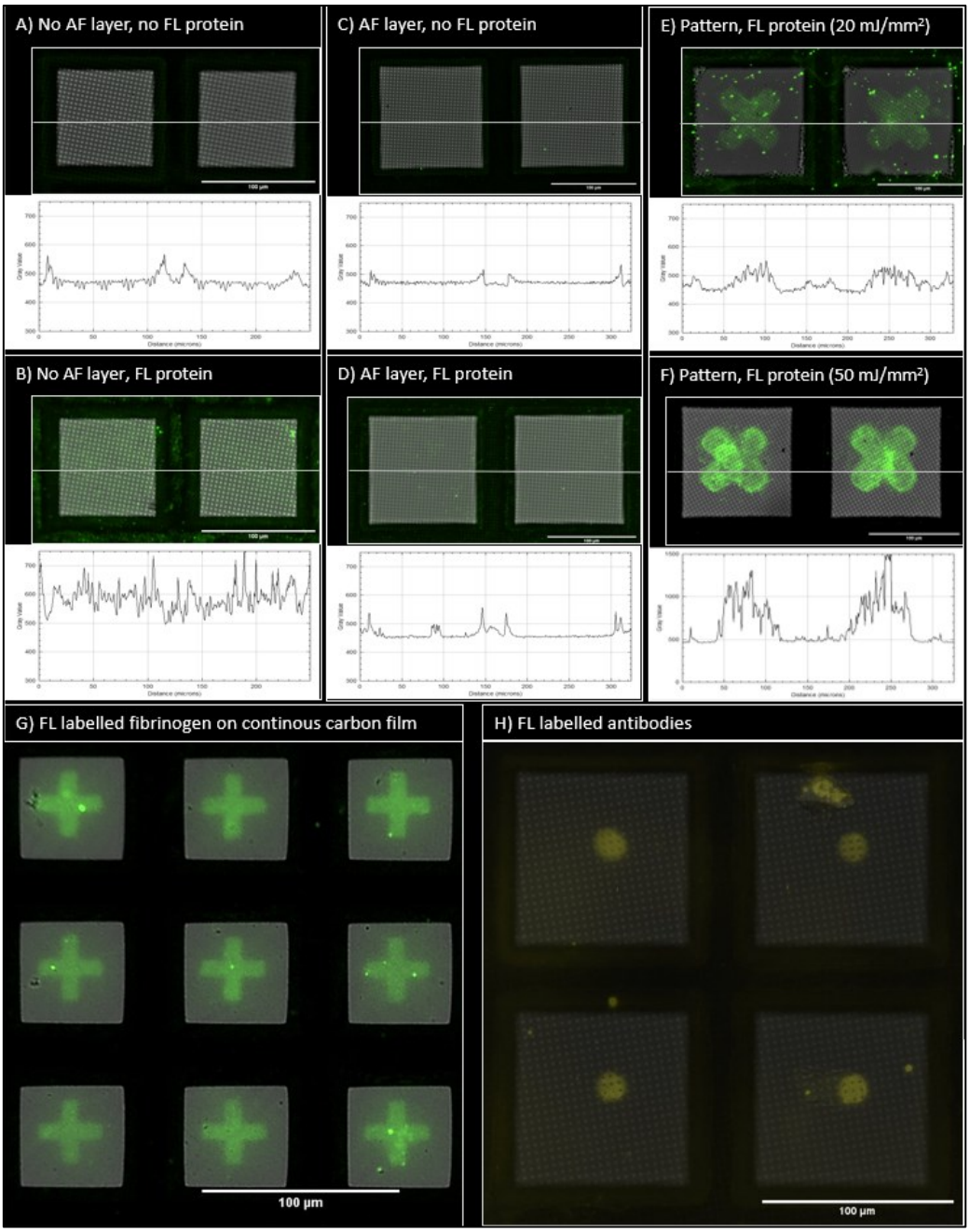

Figure 10: Confirmation of the functionality of the developed protocol with fluorescent signal: ***A)*** *A 200 mesh HC grid with PLL-PEG layer, before the fluorescent fibrinogen was incubated; beneath, the intensity plot over the grey line.* ***B)*** *The same 200 mesh HC grid as in A, after incubating the labelled ECM protein fibrinogen; beneath, the intensity plot over the grey line, indicating an overall increase of fluorescent signal.* ***C)*** *A 150 mesh HC grid with AF layer, before the fluorescent fibrinogen was incubated; beneath, the intensity plot over the grey line.* ***D)*** *The same 150 mesh HC grid as in C, after incubating the labelled ECM protein fibrinogen; beneath, the intensity plot over the grey line, indicating in general no increase of fluorescent signal, except on the edges of the grid bars.* ***E)*** *A 150 mesh HC grid, with AF layer depleted in the shape of cross patterns of 60 µm diameter and 45° tilted relative to the mesh, using 20 mJ/mm² UV exposure. The fluorescent labelled fibrinogen was incubated on the micropatterns. Beneath, the intensity plot over the grey line is shown, indicating a lower fluorescent signal on the AF layer, but about 22% higher fluorescence signal on the patterned area.* ***F)*** *A 150 mesh HC grid, with AF layer depleted in the shape of cross patterns of 70 µm diameter and 45° tilted relative to the mesh, using 50 mJ/mm² UV exposure. The fluorescent labelled fibrinogen was incubated on the micropatterns. Beneath, the intensity plot over the grey line is shown, indicating a fluorescent signal from the AF layer of similar intensity as the AF layer shown in E. The patterned area on the other hand shows a fluorescent signal more than double compared to the patterned area in E.* ***G)*** *A 3x3 grid-square image of a 300 mesh CC grid is shown, to demonstrate that the developed protocol also works when applied on different carbon films. The cross patterns were aligned to the grid bars and have a diameter of about 30 µm.* ***H)*** *A 200 mesh HC grid is shown, patterned with circles of 10 µm diameter. On this grid, a Cy5.5 labelled secondary antibody was incubated, to demonstrate that the developed protocol also works when the grid is functionalized with non-ECM proteins.*

6.1.3 Test different machines to render the grids hydrophilic

2 different machines were tested to evaluate their capability to render the EM grids hydrophilic, a plasma cleaner from HARRICK PLASMA and an ELMO glow discharge system from Cordouan technologies. The grids subjected to plasma treatment from both machines turned out equally hydrophilic and fully applicable for the full micropatterning protocol. No difference could be observed in the B16-F1 melanoma cell behaviour when seeded on the grids. In Figure 11, 2 images from different grids are shown. Both grids were treated with the same protocol, except the system to render the grids hydrophilic in the very beginning. The success of photo patterning was not influenced by the type of machine used in the first step of the developed protocol.

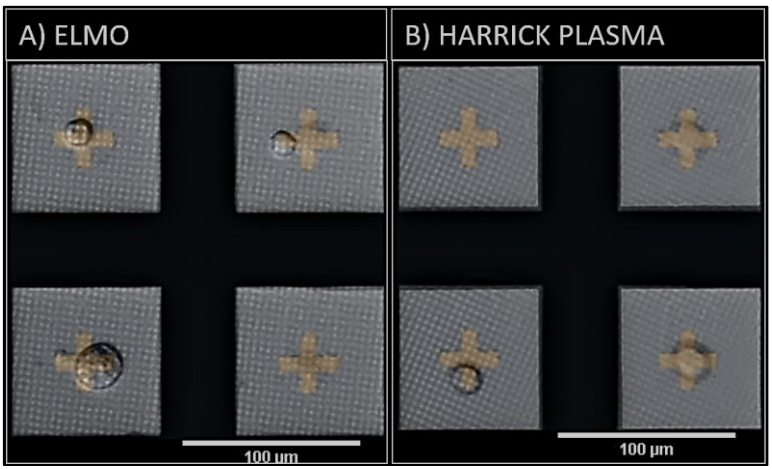

Figure 11: B16-F1 melanoma cells on EM grids: 2x2 grid squares are shown of 2 different grids, submitted to the same protocol for micropatterning, functionalization with laminin and seeding with B16-F1 melanoma cells. The only difference is the machine to render the grids hydrophilic in the first step of the protocol: ***A)*** *the ELMO glow discharge system from Cordouan technologies;* ***B)*** *the plasma cleaner from HARRICK PLASMA. No obvious difference can be seen in regard of the behaviour of the seeded cells and the overall functionality of photo patterning.*

6.2 Evaluating the impact and success rate of photo patterned EM grids for Hela cells

6.2.1 Seeding of HeLa cells on patterned EM grids

To verify the functionality of the described micropatterning protocol on EM grids, HeLa cells were seeded on the processed EM grids, functionalized with laminin. After 2 hours, all cells not adhered to the grid surfaced were washed off, and the cells were imaged in a timelapse of 12 hours, to observe cell behaviour. As displayed in Figure 12 A and B, cells seeded on a grid without AF layer, coated completely with laminin, spread randomly and preferred to stay close or on the grid bars. These cells were considered not accessible for EM experiments. On grids with AF PLL-PEG layer but no UV exposure (C), only a very small number of cells were visible on the grid, and were not able to spread on the carbon layer. In case of micropatterned grids (Figure 12 D to F), cells were almost completely confined to the areas where the AF layer was depleted. 7 hours after seeding (Figure 12 E and F), HeLa cells showed morphological features as on grids without AF layer, but almost exclusively on the patterned areas.

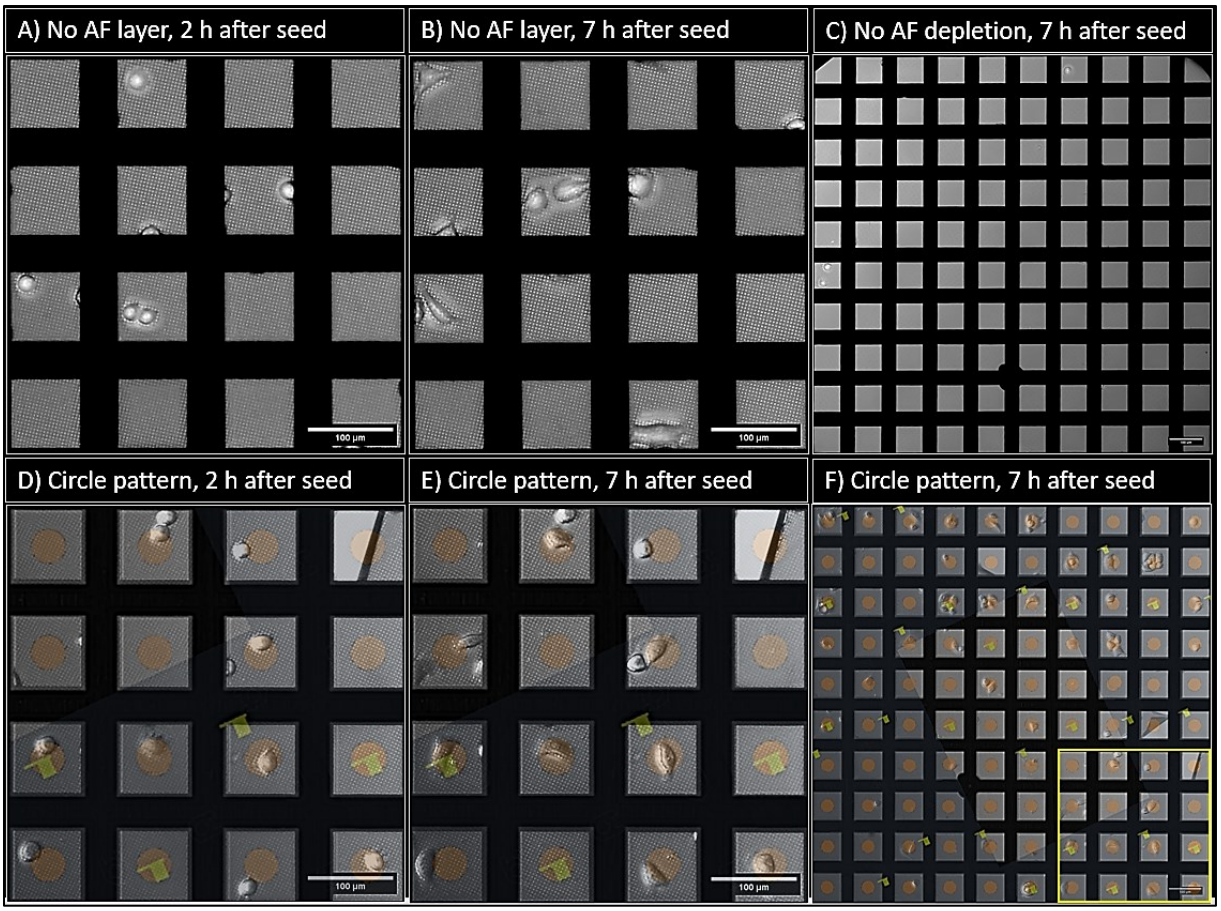

Figure 12: HeLa cells on EM grids: ***A & B)*** *The 2 4x4-square images show the same field of view (FOV) of a 200 mesh Au HC grid coated with laminin* ***(A)*** *after washing off unattached HeLa cells and* ***(B)*** *5 hours after wash off. Visible are cells spreading randomly on the carbon film, preferring on or close to the grid bars.* ***C)*** *A grid coated with PLL-PEG but no AF depletion applied is shown. Only very few cells are visible on the grid, which 7 hours after seeding are not able to spread on the carbon film.* ***D-F)*** *A representative grid is shown where the whole protocol described above was applied. The images were overlain with the photomask displayed by the Leonardo software, to indicate areas with depleted AF layer.* ***D)*** *2 hours after cell seeding, mainly cells attached to the protein patterns are present on the cells.* ***E)*** *7 hours after seeding, the cells spread mainly on the patterns, but not exclusively.* ***F)*** *In the 10x10-square image it is visible that the cells prefer the areas with depleted AF layer, single cells as well as in cell clusters. The yellow square indicates the area shown in more detail in* ***D & E****.*

6.2.2 HeLa cell behaviour on photo patterned grids

HeLa cells, seeded on micropatterned EM grids behaved generally like in a cell culture dish. They attached to the given surface, migrated and spread on it (Figure 13 A and B). At a certain timepoint, an individual cell contracted into a sphere (Figure 13 C) before the cell proliferated, a process observed on grids that takes approximately 50 minutes (Figure 13 D to H). After 2 to 3 more hours, cells again were observed fully spread, or migrated on the sample carrier. The majority of the cells stayed on the laminin patterns, but not exclusively (Figure 13 I). As seen in Figure 13 I in the lower grid square, they were as well able to migrate on the AF layer, but were not able to spread as on the laminin pattern. The possibility of migrating from the protein pattern onto the AF layer is an event rarely observed with HeLa cells. The HeLa cells shown in Figure 13 represented this cell type very well in regard of the timepoint of spreading, as most cells went through the proliferation process approximately 8 hours and 30 minutes after seeding. The very first cell division was observed 6 hours and 20 minutes after seeding, some individuals were observed dividing the first time 12 hours after seeding, at the end of the timelapse experiment (not shown).

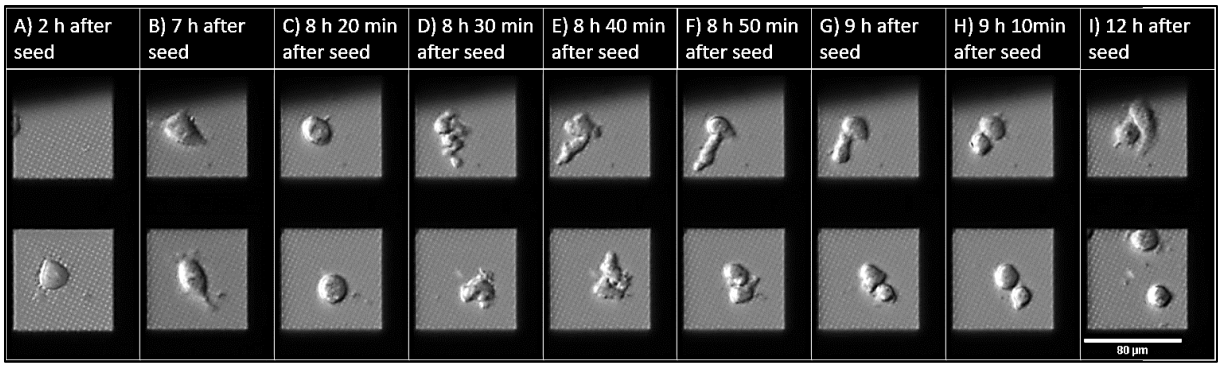

Figure 13: HeLa cell behaviour on photo patterned EM grids: ***A)*** *2 hours after cell seeding, HeLa cells either start to spread on the patterned areas or migrate over the AF layer.* ***B)*** *7 hours after seeding, cells migrated on the available patterned areas and spread fully.* ***C)*** *After about 8 ½ hours after seeding, cells contract to their spherical shape, to proliferate over a course of about an hours* ***(D-H)****.* ***I)*** *About 3 hours after proliferation, cells are fully spread again on the patterned area, or migrate onto the PLL-PEG layer without the possibility to spread due to the AF capability.*

6.2.3 Success rate of micropatterned EM grids with seeded HeLa cells

As shown in Figure 14, on average, 7 hours after cell seeding, 25% of all grid squares contained a single cell in the area applicable for cryo-ET acquisition. 8.3% of the grid squares contained 2 cells. On average, 65% of all grid squares contained more than 2 cells or were empty. With 2000 cells seeded per grid, only a small number of cells were in a spatial position applicable for cryo-ET. The 2 control conditions showed only very little discrepancy in the number of single cells in the centre of a grid square (on average, 2% without AF layer and 1.4% with AF layer), although cells on the AF layer were almost completely prohibited from spreading.

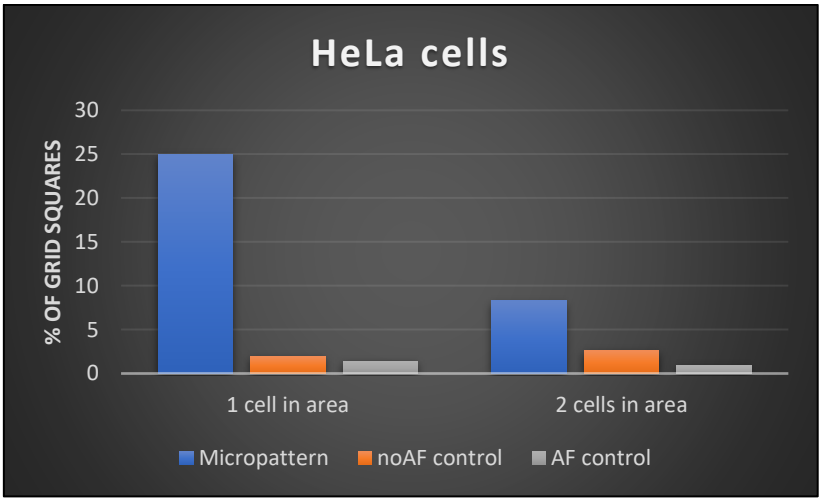

Figure 14: Success rate of optimal placed HeLa cells: On average, 25% of all grid squares contained a single cell optimal positioned for ET workflows, 8.3% contained 2 cells. On the control grids without AF layer, 2% of the grid squares contained a single cell in the centre. On the grids with AF depletion, 1.4% of the grid squares contained a single cell.

6.3 Test photo patterned EM grids with B16-F1 melanoma cells

6.3.1 Seeding of B16-F1 cells on photo patterned EM grids

On grids without AF capacities, B16-F1 cells spread and migrated randomly and preferred the grid bars to adhere (Figure 15 A and B). On grids with a fully intact AF layer (Figure 15 C), most cells were removed from the grid, only a small number of cells were still visible in the grid squares. The cells were to some extend able to spread and displayed morphological features similar to the cell seeded on the grids without AF layer. On grids with areas of depleted PLL-PEG layer (Figure 15 D to F), B16-F1 cells mostly were located on the designated areas, but

not exclusively. Instead, cells migrated on the protein patterns, and were also able to migrate from the patterned area on the bars and to neighbouring grid squares, although they were mostly restricted to the protein patterns for spreading.

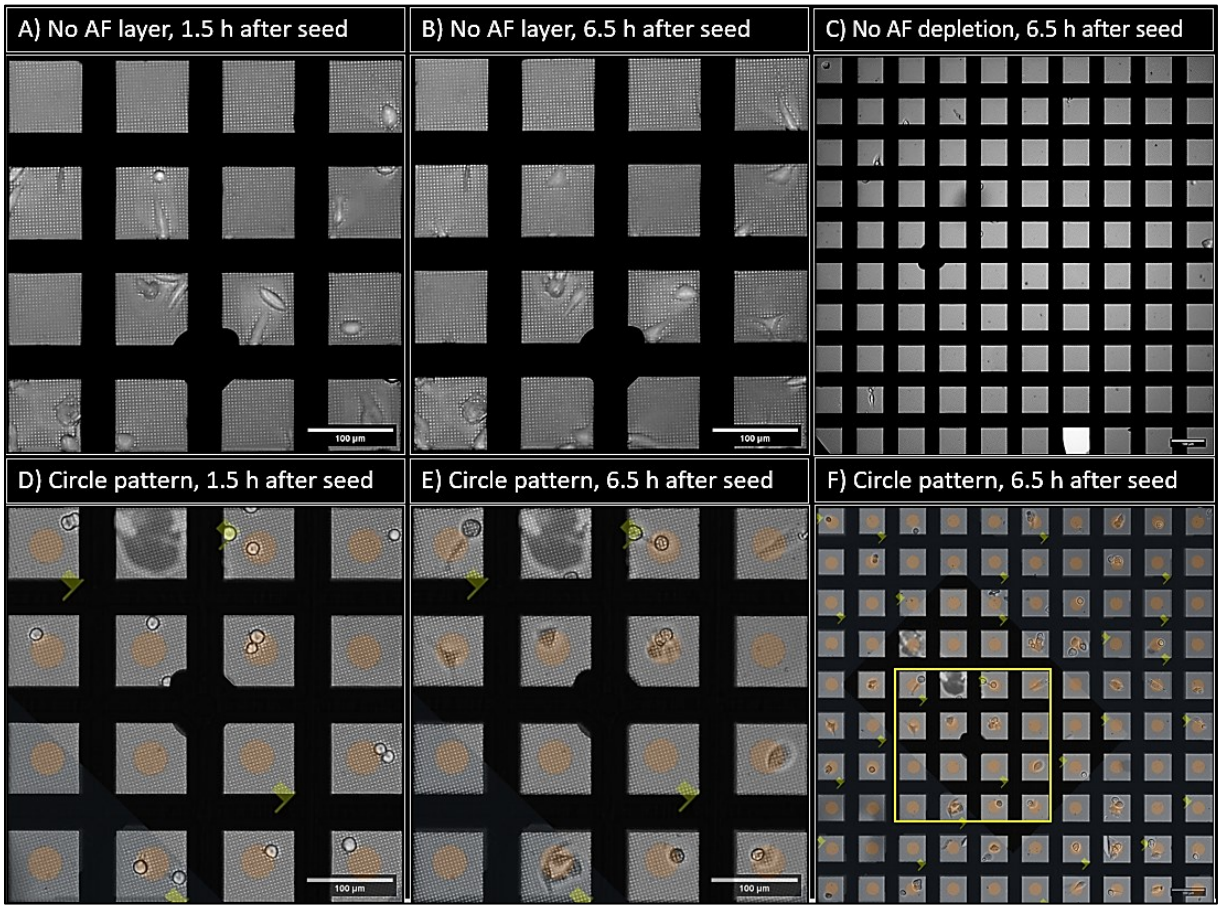

Figure 15: B16-F1 melanoma cells on EM grids: ***A & B)*** *2 4x4-square images of the same 200 mesh Au HC grid coated completely with laminin are shown after washing off unattached B16-F1 melanoma cells, 1.5 hours after seeding* ***(A)*** *and 5 hours after wash off* ***(B)****. Already after 1.5 hours, cells are spreading with uneven spatial distribution.* ***C)*** *A grid coated with PLL-PEG but no exposure to UV light and AF depletion is shown, 6.5 hours after seeding the cells. Significantly less cells are observable on this grid. The B16-F1 cells are able to some extend to spread also on the PLL-PEG layer.* ***D to F)*** *A grid is shown as 4x4 square image where the described protocol with Circle patterns was applied. The photomask from the Leonardo software was used to indicate laminin patterns; the artifact visible in the 2nd square in the top row was present during photo patterning, the square was not recognised as such and no UV light was projected in this square.* ***D)*** *1.5 hours after seeding, most visible cells are located on the protein patterns, though not in a spreading state as in the control grid without AF layer.* ***E)*** *After 5 more hours, cells spread on the patterned areas, showing similar morphologic features displayed by the cells seeded on the grid without the AF layer.* ***F)*** *In the 10x10-square image, the area shown in more detail in the 4x4-square image is indicated as yellow square, and shows the general functionality of the developed protocol for B16-F1 melanoma cells.*

6.3.2 Behaviour of B16-F1 melanoma cells on laminin patterns

After attachment, B16-F1 cells spread on the carbon surface, stretching from the patterned area into the AF layer towards the grid bars (Figure 16 A and B). Individual cells contracted before they divide (Figure 16 C and F), a process that took less than 20 minutes (Figure 16 D and H). Directly after cell division, cells spread again on the protein patterns, staying in close proximity to another. Figure 16 I shows the 2 pairs of divided cells fully spread in close proximity and to some extend stretching into the AF layer. The first cell division was observed already 3 hours after seeding, some individuals were observed dividing the first time 12 hours after seeding, at the end of the timelapse (not shown).

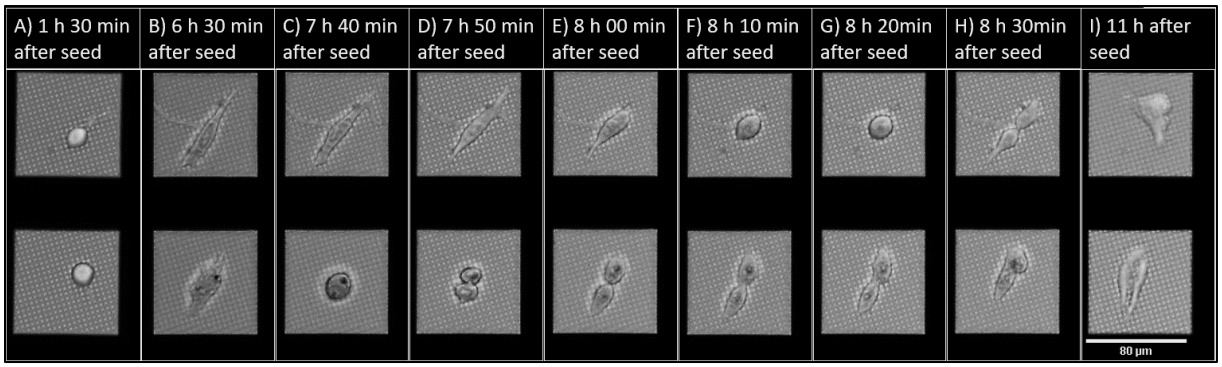

Figure 16: B16-F1 melanoma cell behaviour on photo patterned EM grids: ***A)*** *2 individual cells on grid squares after washing off non-attached cells from the grid.* ***B)*** *6.5 hours after seed, the cells are fully spread on the protein pattern, overlapping to some extend on the AF layer.* ***C-H)*** *The division of both cells is displayed over a timelapse of 50 minutes with 10 minutes interval.* ***I)*** *The same cells 2 ½ hours after cell division, restricted to the protein patterns, again in their fully spread state.*

6.3.3 Success rate of micropatterned EM grids with seeded B16-F1 cells

As shown in Figure 17, on average 5 hours after washing off non-attached cells, 16.1% of all grid squares contained a single cell in the area applicable for cryo-FIB, 4% of all grid squares contained 2 cells in this area. On grids without AF layer, on average 7.4% of all grid squares contained a single cell in the area for cryo-FIB, 2.7% of all grid squares of an EM grid with intact AF layer contained a single cell.

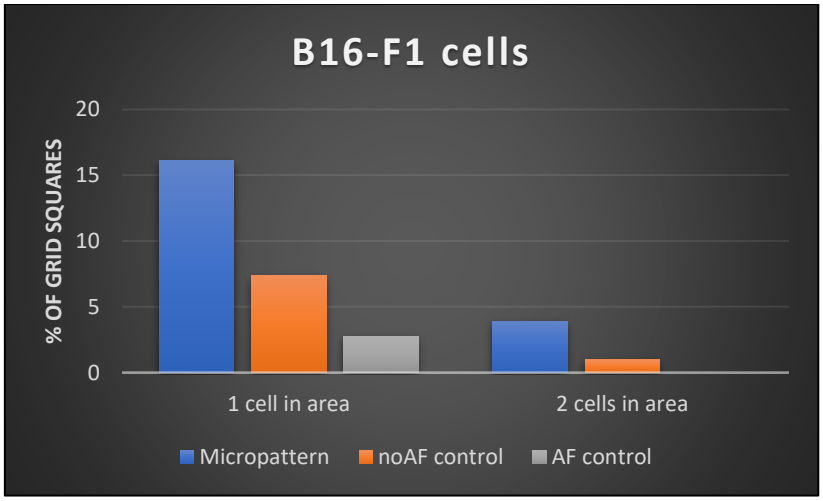

Figure 17: Success rate of optimal placed B16-F1 cells: On average, 16.1% of all grid squares contained a single cell optimal positioned for ET workflows, 4% contained 2 cells. On the control grids without AF layer, 7.4% of the grid squares contained a single cell in the area applicable for ET, on the grids without AF depletion, 2.7% of all grid squares contained a single cell.

6.4 Evaluate the application of the patterned grids for Rat2 fibroblast cells

6.4.1 Cell Seeding of Rat2 fibroblasts

As shown in Figure 18 A and B, on grids without AF layer, Rat2 fibroblasts migrated randomly and preferred to spread in close proximity to the grid bars. On grids with a fully intact AF layer (Figure 18 C), most cells were washed-off from the grid, only a small number of cells were still visible in the grid squares. The cells were not able to spread on this grid. On grids with areas of depleted AF layer in indicated areas (Figure 18 D to F), Rat2 fibroblasts were located almost exclusively on the designated areas. Cells migrated from the AF layer into the patterned regions and tended to stay there over the course of the experiment.

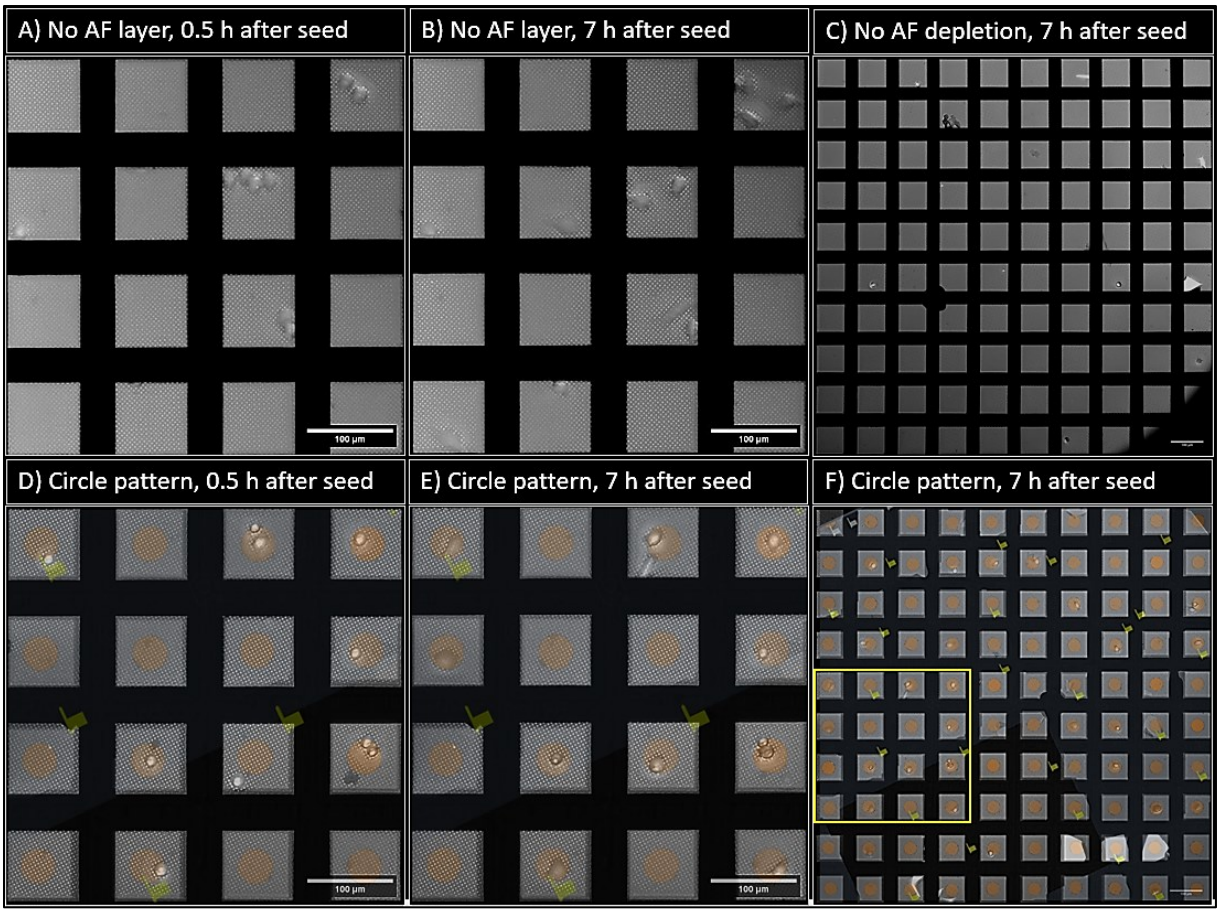

Figure 18: Rat2 fibroblast cell on EM grids: ***A and B)*** *The 2 4x4-square images of a 200 mesh Au HC grid coated with laminin are shown, directly after washing off all unattached Rat2 cells (0.5 hours after cell seeding) and 6.5 hours after wash off (7 hours after seeding).* ***A)*** *After washing off unattached cells, they are already attached to the carbon film randomly, but not spread yet. After 6.5 hours, cells migrated to other, equally random locations on the grid and spread.* ***C)*** *A grid coated with PLL-PEG but no AF layer depletion is shown 6.5 hours after washing off all unattached cells. Less cells are observable on this grid compared to the grid representing a grid without PLL-PEG layer.* ***D to F)*** *A grid is shown where the described protocol with Circle patterns was applied, with patterned areas indicated with the Leonardo photomask.* ***D)*** *After wash-off of unattached cells, most cells visible are located on the protein patterns.* ***E)*** *Cell spreading was almost exclusively limited to the patterned areas. Also visible is the migration of the cells from the AF layer onto the patterned areas.* ***F)*** *Shown in the 10x10 grid-square image is the general functionality of the patterning strategy. The area of the grid used for the 4x4-square image is indicated with the yellow square in the 10x10-square image.*

6.4.2 Rat2 cell behaviour on laminin patterned EM grids

Rat2 cells attached very fast to the carbon film of the EM grid and migrated on the AF layer and the protein patterns. They were almost completely restricted from spreading on the AF layer. They were able to spread on a patterned area as soon as they migrated there from the AF layer (Figure 19 A). Nevertheless, they neither spread quickly (Figure 19 B) or proliferated at a high rate, only a small number of cells divided at all over the course of the timelapse experiment. Before cell division, Rat2 cells contracted to a spherical shape, the whole process took about 40 minutes (Figure 19 C to F). In the following, the cells continued migrating on the protein pattern, but tended to not leave the patterned area (Figure 19 G, H and I).

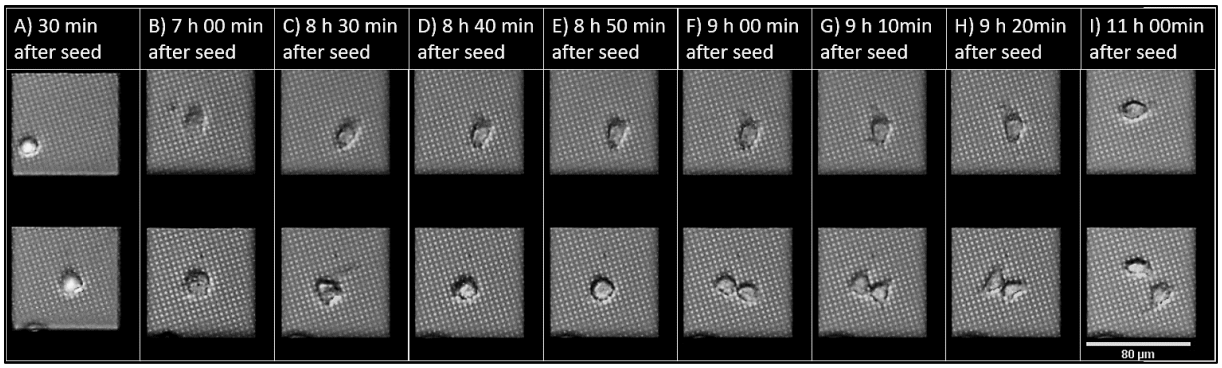

Figure 19: Rat2 fibroblast cell behaviour on photo patterned EM grids: ***A)*** *Individual Rat2 cells on 2 grid squares, directly after washing off non-attached cells.* ***B)*** *7 hours after seeding, both cells are located on the protein patterns and in a spread state.* ***C-E)*** *8 ½ hours after cell seeding, the cell on the lower grid square starts retracting and form a sphere, this process takes about 30 minutes.* ***F-H)*** *The cell divides, the individual cells migrate independently on the protein pattern.* ***I)*** *11 hours after cells seeding and 2 hours after cell proliferation, the cells stay confined on the protein pattern. They did not migrate onto the AF layer.*

6.4.3 Evaluation of the success rate for Rat2 fibroblasts

In Figure 20, the distribution of Rat2 fibroblast cells on micropatterned grids compared to both control conditions is described. On average, 21.6% of all grid squares contained a single cell in the area applicable for ET acquisition, while 4.9% contained 2 cells. On the control grid without AF layer, 8% of the grid squares contained a single cell in this area. On the grid with AF PLL-PEG layer without UV depletion, only 2% contained a single cell in the designated area.

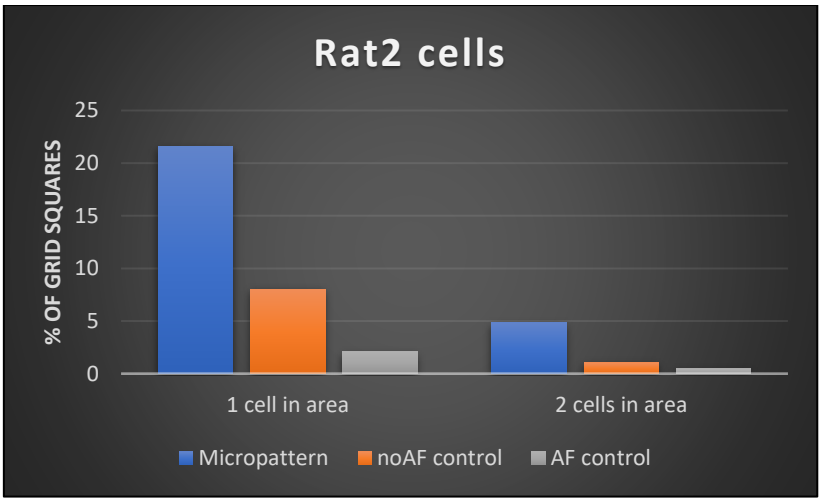

Figure 20: Success rate of optimal placed Rat2 cells: On average, 21.6% of all grid squares contained a single cell optimal positioned for ET workflows, 4.9% contained 2 cells. On the control grids without AF layer, 8% of the grid squares contained a single cell in the area applicable for ET, on the grids without AF depletion, 2% of the grid squares contained a single cell.

6.5 Control Cell behaviour with pattern shapes

6.5.1 HeLa cell behaviour on different pattern shapes

Compared to the circle patterns (Figure 21 A), HeLa cells on dumbbell patterns (Figure 21 B) either stretched over the whole pattern. This behaviour was highly repetitive over the whole grid. On the cross shape (Figure 21 C), cells spread mostly over 3 of the four available arms, though not exclusively; this cell behaviour was as well highly repetitive. On the fan shaped patterns (Figure 21 D), cells were restricted to the protein pattern and therefor had difficulties spreading due to the limited area available. Also, cells on this grid appeared in more clumps than on the other grids, although all of the shown grids with dumbbell, cross and fan shape were prepared in the same biological replicate from the same cell dilution. On all patterns,

HeLa cells used the area available for spreading as much as possible, in case of bigger protein patterns (the dumbbell and cross patterns), cells tended to stretch and avoided the AF layer. On the smaller fan pattern, cells tended to stay in their spherical shape, as not enough area was provided for them to spread. All images shown in Figure 21 display HeLa cells 7 hours after seeding.

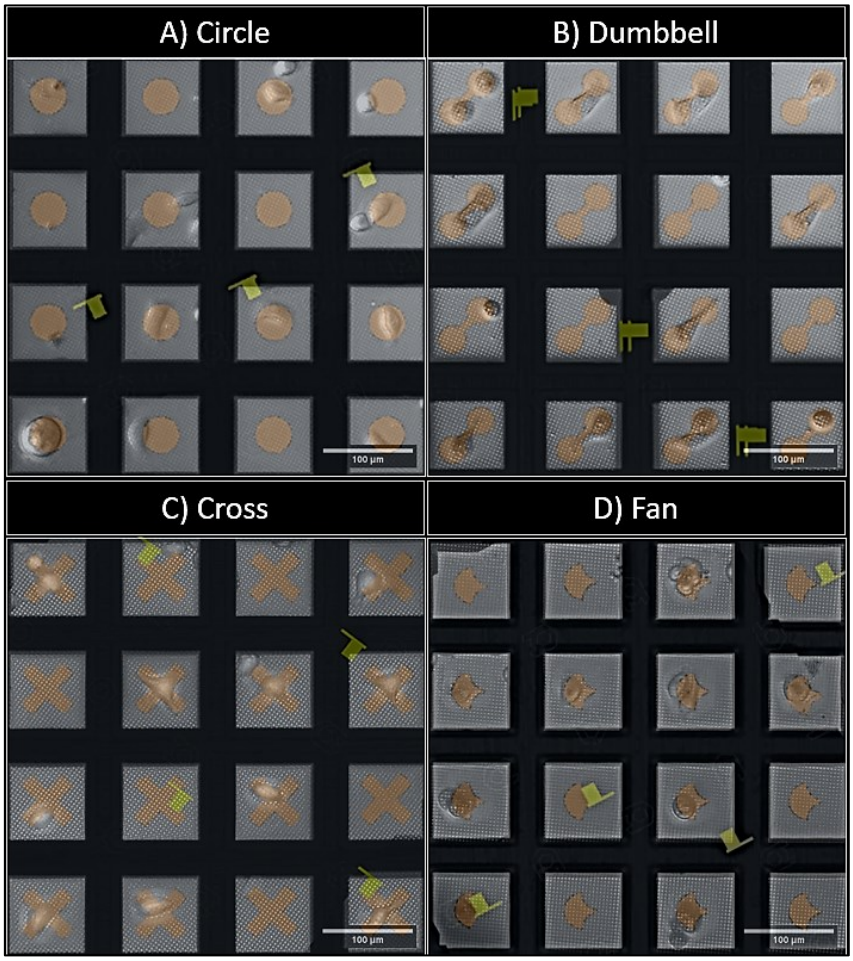

*Figure 21: Hela cells on different pattern shapes: 8x8 grid squares of grids with different pattern shapes are shown, 7 hours after seeding referring to 5 hours after wash-off of unattached cells. The grids were beforehand subjected to the full protocol developed in this work. Circle- and fan-shaped patterns have a diameter of 40 µm, dumbbell- and cross-shape patterns a diameter of 60 µm. All images were overlain with the photomask displayed by the Leonardo software for photopatterning to indicate areas coated with depleted AF layer. On all shapes, cells are mostly confined to the patterned areas. On dumbbell and cross patterns **(B and C)**, as more space is available for attachment, the cells tend to spread wider than on the smaller fan patterns **(D)**. The cell morphologies are highly repetitive.*

6.5.2 B16-F1 melanoma cells on different pattern shapes

As this cell type is prone to migrate on the surface it is adhered to and chance its morphological features in that process, the cell shape was less constant than from the former described HeLa cells. Despite more available surface for attachment on the dumbbell patterns (Figure 22 B) compared to the other three patterns, cells tended not to stay in their spread shape; instead, they repeatedly stretched over the thin bridge to retract again into a spherical shape rhythmically, jumping from one of the circular regions to the other. Although the patterned areas were preferred by the cells, they were able to leave the patterned regions and migrated over the antifouling layer towards the grid bars, to eventually migrate back on a patterned area. The pattern of small crosses (Figure 22 C), cells were more restricted from migration onto the AF layer; they tended to stretch over the whole pattern and contracted again rhythmically, a behaviour highly replicable over the whole grid and over multiple replicates. The fan-shaped

pattern (Figure 22 D) seemed to have the least obvious effect on the resulting cell behaviour and morphology, B16-F1 cells adhered on it and migrated in it, stretched over the edge into the AF layer and contracted again.

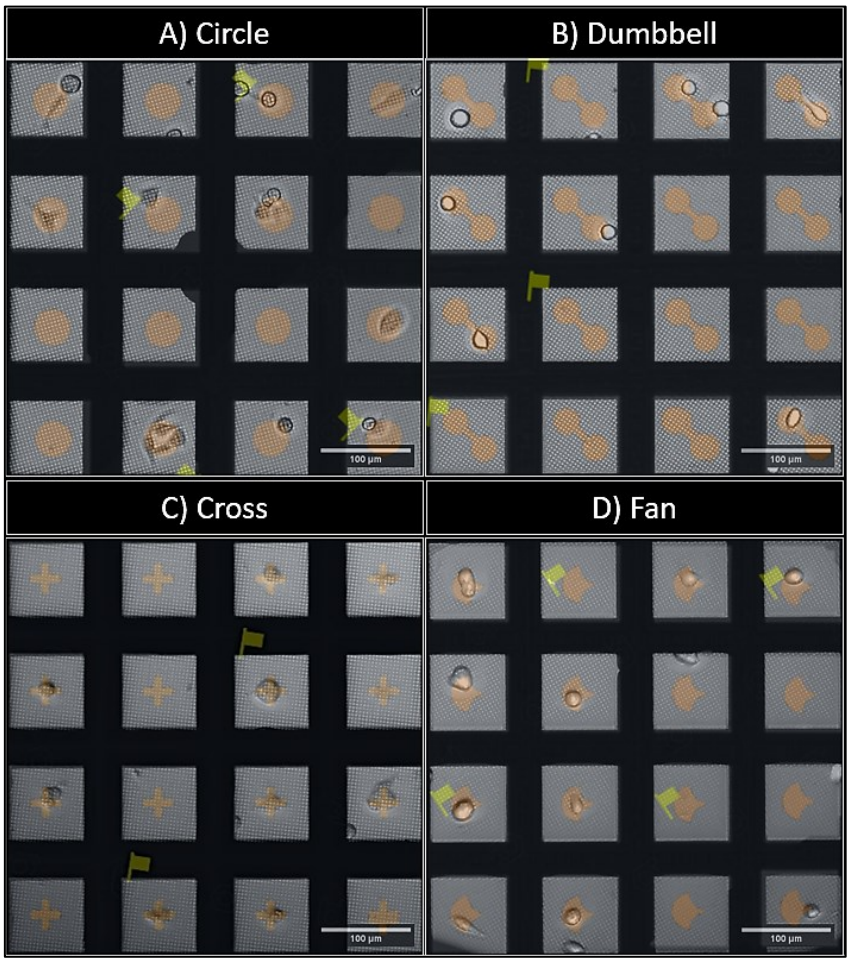

*Figure 22: B16-F1 melanoma fibroblast cells on different pattern shapes: 8x8 grid squares around the centre of the grid are shown. The grid was beforehand subjected to the full protocol described above; circle- **(A)**, cross- **(C)** and fan- **(D)** shaped patterns have a diameter of 40 µm, dumbbell-shaped patterns **(B)** a diameter of 60 µm. All images show B16-F1 melanoma cells 6.5 hours after seeding, 5 hours after washing off non-attached cells. All images were overlain with the photomask displayed by the Leonardo software for photo patterning to point out the areas coated with the ECM protein laminin. On the dumbbell patterns **(B)**, cells only spread in the direction of the patterns.*

6.6 Rat2 fibroblast cells

Similar to HeLa cells, on the dumbbell patterns (Figure 23 B) Rat2 cells tended to stretch the circular structure over the thin bridge to the other circle, though the behaviour was less replicable as with HeLa cells. In many cases, the cells started to stretch only to contract again into circular cell shape. On the cross patterns (Figure 23 C), a lot of patterns were occupied with 2 cells after seeding. The Rat2 cells stretched over the patterned area and retracted again to their spherical shape. The least obvious cell behaviour could be read out when seeding Rat2 cells on grids with fan shaped patterns (Figure 23 D). Cells stayed in their spherical shape in most cases. Further, similar to HeLa cells, many cell clumps were visible on this grid, despite their preparation in the same biological replicate as the other patterns and usage of the same cell dilution.

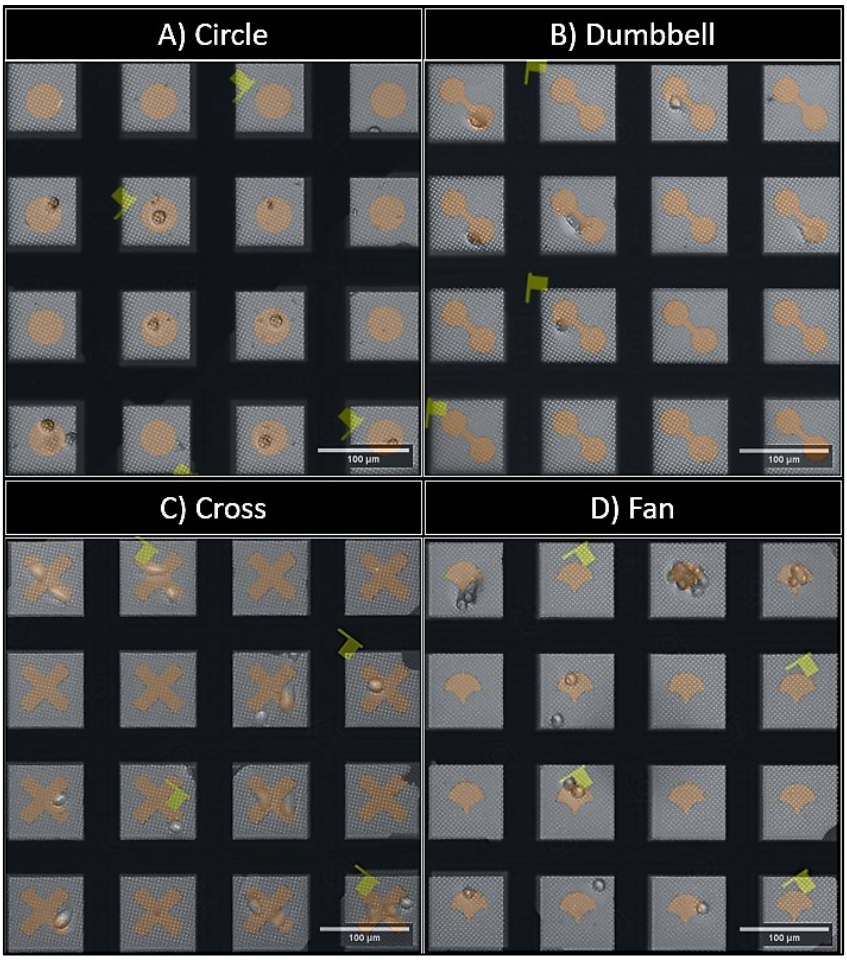

*Figure 23: Rat2 fibroblast cells on different pattern shapes: 8x8 grid squares of the grid are shown. The grid was beforehand subjected to the full protocol described above; circle- **(A)** and fan- **(D)** shaped patterns have a diameter of 40 µm, dumbbell- **(B)** and cross- **(C)** shape patterns a diameter of 60 µm. All images show Rat2 fibroblasts 7 hours after seeding, 6.5 hours after washing of non-attached cells. All images were overlain with the photomask displayed by the Leonardo software for photo patterning to highlight the regions coated with laminin patterns. In all 4 cases, Rat2 cells prefer the patterned area over the surrounding AF layer, and barely migrate out of these regions. Cell morphologies are highly repetitive between patterns of the cell shape, on the dumbbell and cross patterns with bigger protein area available **(B and C)**, they tend to spread to full extend, while on smaller areas of the fan-shaped patterns **(D)**, they tend to stay in the spherical shape.*

6.7 Problems & difficulties observed while performing the photo patterning protocol on EM grids

6.7.1 Bubbles in photo initiator

The PLPP gel photo initiator tended to contain air bubbles when repeatedly used. These bubbles couldn't diffuse out of the gel over time due to the viscosity of the gel. To get rid of them, the initiator had to be diluted and mixed in ethanol. Otherwise, the bubbles in the initiator applied on the EM grids adhered to the carbon film and impacted the patterning process negatively, by either restricting the individual grid squares from detection with the EM grid wizard in the Leonardo software (shown in Figure 24), or by reflecting the UV light uncontrolled. It should be noted, that these bubbles formed also when the grid was bended and the initiator was sucked between the EM grid and the glass surface.

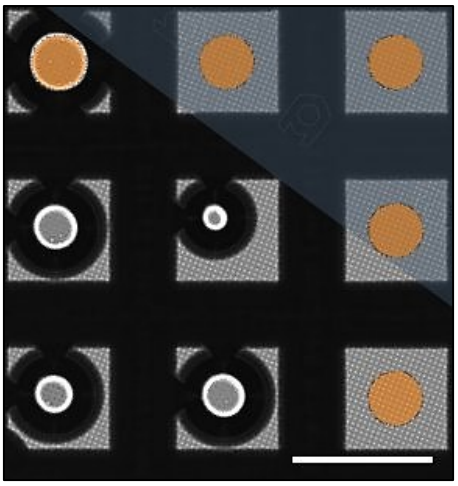

Figure 24: Bubbles trapped under the EM grid: PLPP gel not diluted with ethanol can contain air bubbles; these air bubble can restrict the grid square from detection with the EM grid wizard (no pattern placed), or negatively influence the projection of UV light, as the light gets scattered uncontrolled by the air bubble. The bubbles can also form, when the grid coated with PLPP gel is flipped prior to patterning. The scale bar is 100 µm in size.

6.7.2 Scattering of UV light in the PLPP photo initiator

Light, when interacting with a sample in solid, liquid or gaseous state, can be reflected, transmitted, absorbed or scattered. When the UV light was projected by the DMD towards the EM grids coated with the PLPP photo initiator, the light was scattered by the initiator, resulting in a longer wavelength collected by the objective, able to pass the dichroic mirror and recorded by the camera (see Figure 25 A & B). Visible in Figure 25 B, the UV light was to some extend also reflected in the photo initiator towards the edges of the grid squares.

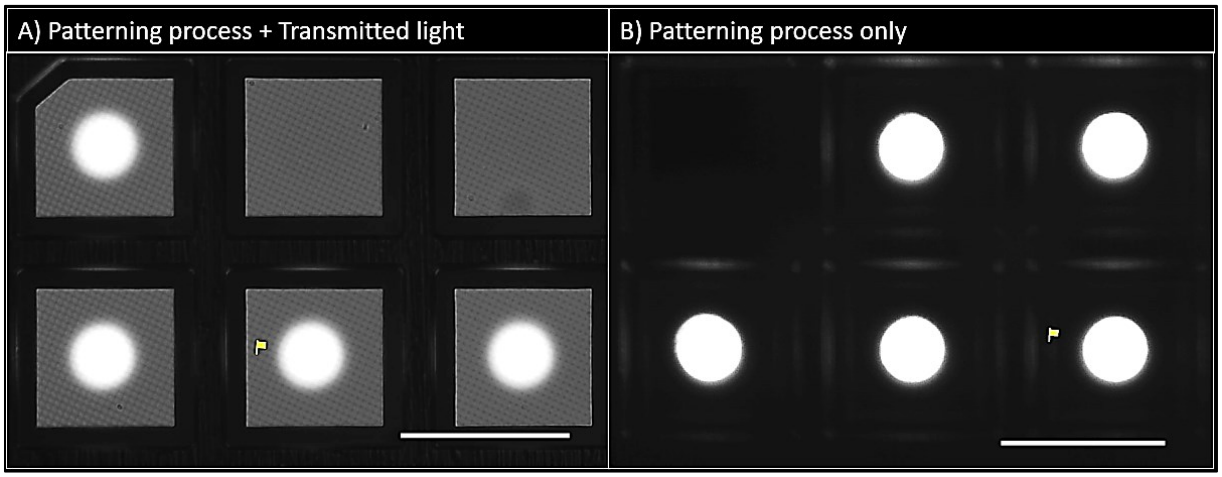

*Figure 25: Scattering of UV light in the photo initiator: **A)** The photo patterning process on a 200 mesh HC grid, in combination with transmitted light to show the grid; the white circles result from UV light scattered by the PLPP gel and detected by the camera. **B)** The same grid at a different position, shown without transmitted light channel; the dim white lines at the edges of the grid squares result from light reflected in the photo initiator and scattered at the edges of the grid square. This reflected light might be able to activate the photo initiator to a small extend and digest the AF layer on the edges of the grid squares. Scale bars are 100 µm in size.*

6.7.3 The importance of the number of cells seeded

Cells seeded on micropatterned EM grids were as individuals in most cases not able to adhere and spread on the AF layer coating the area outside the protein patterns. Nevertheless, if the number of seeded cells was too high, cells were able to adhere to each other, bypassed the AF capability of the grid and spread on the PLL-PEG layer (Figure 26 A). If the cell number is too low, the amount of spatial positioned cells applicable for ET acquisition is reduced. The evaluated number of seeded cells per processed grid was evaluated by seeding 500, 1000,

2000, 5000 and 15000 cells on different grids in one biological replicate. The proposed number of 2000 cells seeded had the highest success rates for all cell types.

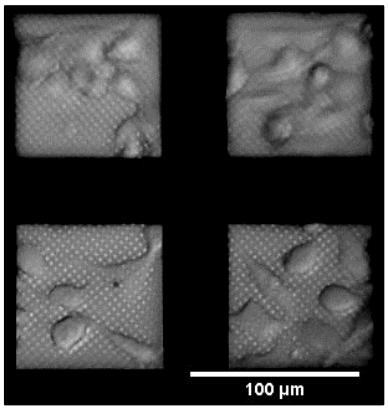

Figure 26: Too many cells seeded on a photo patterned grid: Cell are normally not able to adhere to the AF layer. If the number of seeded cells is too high, they are nevertheless able to spread on the PLL-PEG layer, as the cells also are able to attach to each other.

6.7.4 Wash-off of unattached cells

The wash-off strategy was performed on EM grids in grid holders placed in a 96 well-plate, and came with 2 problems, displayed in Figure 27: i) when the fresh cell-culture medium was pipetted onto the grid, cells weren't removed from the carbon film reliably. Instead, many cells were pushed to the edges of the grid (Figure 27 A) where they formed cell clusters (Figure 27 B). ii) During the wash-off procedure, the fresh medium was pipetted into the liquid on top of the grid to remove the non-attached cells and the same volume of medium was removed again from the well of the well plate. This did not remove all cells floating in the medium. Instead, individual cells were floating in the well, eventually sinking down again on the grid shortly after the wash-off (Figure 27 C).

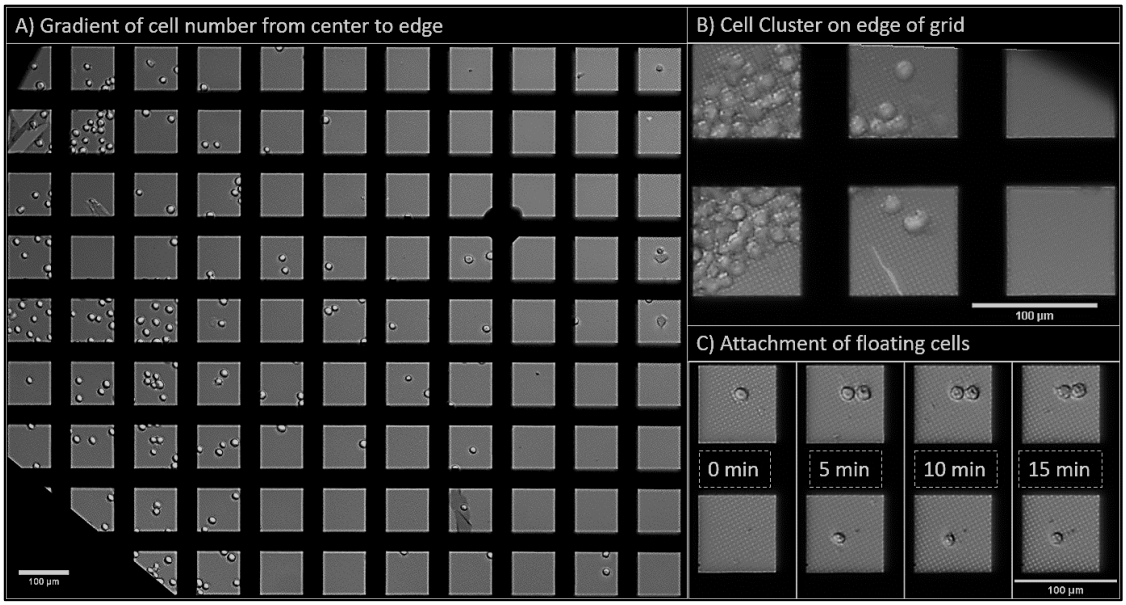

*Figure 27: Important facts regarding washing off cells from grid: **A)** The increasing number of cells on the grid is shown directly after washing off unattached cells. While close to the centre, cells are mainly attached to the protein patterns, cells accumulate on the edge of the grid. **B)** A cluster of many cells is shown, formed after washing off unattached cells and pushing them together at the edge of the grid. **C)** A timelapse with 5 minutes interval shows the spontaneous appearance of 2 cells in the patterned areas of 2 squares, directly after washing off unattached cells. No migration is observed of those cells in the following frames, making it unlikely that those cells migrated on those grid squares from the AF layer. Instead, those cells probably sank down to the carbon surface after wash-off and attached in these grid squares.*

7 Discussion

7.1 Photo patterning of EM grids

The key findings during the protocol development and culturing of different cell types on laminin patterned EM grids were: i) using photo patterned EM grids leads to an increase of three to five times the number of individual cells in a spatial position applicable for eventual ET experiments, dependent on the cell type. ii) The protein pattern quality can be maintained while the amount of time for grid preparation is reduced to a few hours, and the use of expensive reagents is minimized. The developed protocol was shown to be applicable to different carbon coatings on the EM grids, and proteins apart from ECM proteins. iii) EM grid holders, as they are manufactured now, are not applicable for the micropatterning process iv) Different cell types behave different in regard to their attachment to the grid surface, in their migration and proliferation on the laminin patterns as well as on the AF layer. v) The cell morphology can be manipulated easily by changing the protein pattern shape, and their behaviour depends mostly on the pattern shape and not on the area of the protein patterns.

Below, I will again discuss the main steps in performing photo patterning on EM grids using the PRIMO micropatterning system and point out possible improvements. I will compare the success rate and behaviour of the three cell lines on micropatterned EM grids, and point out the important factors for eventual subsequent preparation for EM experiments. Finally, I will compare the developed strategy to other protocols published in the last years, and evaluate the advantages and shortcomings.

7.1.1 i) Reduce grid bending and carbon film tearing

As the HC film can easily tear when drying in contact with a surface [39], the protocol involves drying steps only either in a vertical position in EM grid boxes, or placed on glass surfaces with the carbon film-side facing upwards. The photo patterning with the PRIMO system was performed by projecting the UV light directly through the carbon film, instead of flipping the grid prior to it. This strategy not only reduces the risk of damaging the grid by moving it with tweezers, but additionally the thickness of PLPP photo initiator does not have an influence on the pattern quality. Only the thickness of the carbon film needs to be taken into account.

7.1.2 ii) Reduce uncontrolled PLL-PEG digestion

As soon as the photo initiator was applied onto the grids, they were kept in the dark, protected from ambient light, to avoid activation of the initiator and digestion of the AF layer. To further reduce unwanted activation of the photo initiator, the transmitted light of the microscope was turned off after the whole grid was imaged with a transmitted light tiled image. The exposure to the 365 nm LED light was reduced to minimum of 50 mJ/mm^2, a value evaluated to be sufficient to digest the AF layer, but minimize the time in which UV light is reflected by the PLPP gel. It has to be mentioned at this point, that the photo scission reaction of the AF layer (shown in Figure 3 C) is performed by the initiator at random points in the PEG chain. Too short exposure times might lead to an unreliable AF depletion and in the following to randomized ECM protein concentrations between patterns.

7.1.3 iii) The application of EM grid holders for photo patterning and cell culture

The usage of 3D printed grid holders has several advantages in the grid preparation steps following the photo patterning procedure, starting from the rehydration of the AF layer and the functionalization of the patterns with proteins. The number of cells required to have enough individual cells adhered on the EM grid is reduced compared to other strategies, also reduced is the necessity to move grids with tweezers as soon as they are placed in the holders. Concluded, the use of materials and reagents can be reduced, as well as the number of required cells. Also, the transport of the grids is facilitated. [63]

Nevertheless, testing the patterning procedure directly in the EM grid holders did not work, due to two issues: i) when the diluted photo initiator is applied on the grid, mounted in the grid holder, it is sucked from the grid into the narrow gap between grid and holder due to capillary forces; ii) as the 3D-printed grid holders don't hold the grids in a nearly perfectly flat position, due to small irregularities in their structure, the focus on the HC film is not sufficient over the whole area. Subsequently, the grid square detection and patterning procedure cannot be performed properly. Nevertheless, if only a small area is required to be patterned, e.g., the central 6x6 grid squares around the centre, the tilt of the grid can potentially be small enough to have sufficient focus on this region. It is unclear, if specific calibrations of the micropatterning system are required, due to the distance between cover slip and carbon film.

The grid holders tested in this work were manufactured using the fused deposition modelling (FDM) method [63]. This is the most commonly used 3D printing method for plastic filaments. FDM works by depositing molten plastic filament layer by layer through a heated nozzle onto a build platform to create the prior designed object [66]. The filament is typically made of materials like polylactic acid (PLA) or acrylonitrile butadiene styrene (ABS). Glycol-modified polyethylene terephthalate (PETG) was used to produce the EM-grid holders due to its bio-compatible properties [63]. FDM printers offer relatively lower precision compared to other methods, as they have limitations in achieving fine details and smooth surfaces [67].

To improve the quality of the 3D-printed grid holders, a printing technique with higher resolution has to be applied, like Stereolithography (SLA). In this technique, a liquid resin as the raw material is used. A UV light sources selectively solidifies the resin layer by layer to create the desired object [67]. SLA printers can achieve higher precision and finer details compared to FDM. SLA in general results in a higher object resolution, smoother surfaces and offers the possibility of more complicated and detailed designs [67].

7.1.4 iv) Functionalization of the micropatterns

For the functionalization of the EM grids with ECM proteins, two factors are important to mention: i) the concentration of the protein in dilution and ii) the incubation time of the grids in the protein solution. In literature, most protocols use an ECM protein concentration of 25-100 µg/ml and an incubation time of 30 min-1 hour (see Figure 28). Those values can further be optimized to reduce the amount of reagents and time for sample carrier preparation, but are shown in this work to function reliably for the purpose of cell attachment to the carbon film.

7.1.5 v) Cell seeding

The number of cells to be seeded on micropatterned EM grids mounted on grid holders in a 96-well plate were in this work evaluated to maximize the number of grid squares occupied by a single cell. If too many cells are seeded, the grid squares tend to be overcrowded, if too little cells are seeded, the number of empty grid squares increases. Further, the volume of cell dilution used for seeding impacts the outcome. If the same number of cells is seeded from a smaller volume and with a smaller pipette tip, the cells tend to be located on the same region of the grid and to form cell clusters. For those reasons, a cell dilution of $1.5x10^5$ cells/ml was prepared for seeding, and 13.3 µl of it were used, resulting in 2000 cells seeded onto each grid. The preparation of Rat2 fibroblasts was performed slightly different than those for HeLa cells and B16-F1 cells, as Rat2 cells immediately start to attach to any surface, when the trypsin in the cell culture medium is deactivated by bovine serum. Therefore, the trypsin used in the cell culture dish containing the Rat2 cells was not deactivated before the cell count was performed, only when the cell dilution was prepared, which was immediately used to seed Rat2 cells on the EM grids. Such cell-specific differences in the procedure for cell seeding need to be kept in mind, when explored for other cell types.

Depending on the size of the protein pattern areas, it was assumed in the beginning of the project that the number of cells also has to be evaluated, to avoid adhesion of multiple cells to

the same grid square. Nevertheless, the sizes of the areas do not correspond to the success of single cells attached to the patterns. Instead, the pattern shape seems to be the deciding factor on the successful adhesion of a single cell to a protein pattern.

7.1.6 vi) Wash-off of non-attached cells

As cells after seeding sink down on the EM grid and need some time to adhere to the carbon film, different cell lines require different times until a wash-off of non-attached cells can be performed, to avoid removal of cells from the protein patterns. For all three cell lines used in this work, this timepoint was evaluated and the optimal timepoint stated. While the wash-off strategy described here works in principle to remove cells from the AF layer, the location of the grids in the grid holder and further in the 96-well plate comes with two difficulties: i) the collection of cells in clusters at the edge of the grid and ii) the location of the washed-off cells floating in the liquid above the grid, not removed by extracting excessive culture medium from the well.

Cells washed off the AF layer and collected at the edges of the grid are potentially able to migrate on the AF layer. They have the potential to migrate towards the centre of the grid and subsequently on a protein pattern already occupied by a single cell. This can lower the success rate of individual cells placed in a spatial position to subsequently fix the cells and perform ET acquisition. The cells floating in the cell culture medium have the potential to sink down again on the carbon film and adhere to it. This can only be avoided by removing all of the cell culture medium from the well and refilling it with medium. This strategy nevertheless induces the risks of misplacing of the grid in the grid holder, disrupting the AF properties exposure of the PLL-PEG layer to air or the introduction of air bubbles under the grid.

Both issues described can have a positive or negative impact on the success rate of the spatial placement of individual cells, as the cells migrating on the carbon surface as well as the floating cells can either attach to an empty grid square, or to a square already occupied by a single cell. As these problems cannot be controlled by performing the protocol described in this thesis, the wash-off procedure would need further optimization.

7.2 Compare success rates between cell lines:

The success of the photo patterning protocol described in this work was evaluated by counting grid squares occupied by a single cell, placed in a position applicable for downstream ET acquisition. The success rates depended strongly on the cell type, and their differing potential to migrate on the carbon surface and especially from the patterned area onto the AF layer. While HeLa cells and Rat2 fibroblasts are in general highly confined by the protein patterns, B16-F1 cells were observed more often to leave the patterned areas and migrate onto the AF layer. Hence, the evaluated success rates differ: while HeLa and Rat2 cells had a success rate of 20-25% on average, B16-F1 cells only had a success rate of about 16%. What further decreased the success rate of B16-F1 cells compared to the other two cell types is the fact, that HeLa cells started to divide relatively late on EM grids, and Rat2 cells barely proliferated at all. B16-F1 cells on the other hand already started after 3 hours, if both of the cells over the course of the time observed stayed on the grid square, it was not counted successful as not an individual cell was located in this square.

7.3 Cell behaviour

Different photo masks were drawn in Inkscape and integrated into the Leonardo EM grid wizard to be projected by the PRIMO 2 system onto the EM grids and to initialize the digestion of the AF layer. The processed grids were treated equally, laminin was used for pattern functionalization on all grids and cells were seeded in the same number, the only difference was the cell line. The behaviour of the cells was narrowed down to the three factors cell spreading, cell migration and cell proliferation.

7.3.1 HeLa cells

HeLa cells were almost exclusively restricted from spreading outside of to the protein patterns. They were able to migrate in rare events from the patterns onto the antifouling layer and towards the grid bars. Most migration events observed were from the AF layer onto the protein patterns. HeLa cells proliferated only on the patterned areas, by changing their morphology from the spread form into the contracted spherical form, followed by duplication and again spreading on the pattern. As HeLa cells used as much of the patterned area as possible, they followed the pattern shapes in great detail, visible especially in the case of the dumbbell and cross patterns. In case of the fan-shaped pattern, cells seemed to be unable to spread to full extend, as the area provided was relatively small. If downstream EM acquisition is planned with HeLa cells seeded on micropatterned EM grids, the optimal timepoint for fixation according to the findings shown here is about 7 hours after cell seeding, to avoid cell doublets due to cell proliferation, but having the cells in their fully spread form.

7.3.2 B16-F1 cells

Compared to HeLa cells, B16-F1 cells were able to some extent to spread also on the PLL-PEG layer. They stayed in their stretched, spindle-like morphology despite the pattern shape. They were further able to migrate from the protein pattern onto the AF layer, although the protein patterns seem to be preferred for spreading. They were not observed to spread to full extend along the grid bars, as it was the case in the control grid without AF layer. Cell proliferation was only observed on protein patterns. Similar to the behaviour of the other cell lines, they first contracted into a sphere, before dividing and spreading again. The whole process took less time than in the case of the HeLa or Rat2 cell types, in most cases less than 20 minutes. Compared to the control grid without AF layer, and also compared to the other cell types, B16-F1 cells did not stay in their spread state for long. Instead, they contracted and spread again, stretching not only over the whole protein pattern but in some cases over the whole grid square, spanning from bar to bar. They nevertheless followed the patterns in regard of the orientation. On the dumbbell patterns, they stretched along the axis of the pattern, between the corners of a grid square. From the data acquired for this work, an approximate timepoint of cell division cannot be estimated, as division events were not concentrated at a certain timeframe, but instead distributed over the whole course of observation after the wash-off procedure. Therefore, a timepoint optimal for eventual fixation could not be evaluated.

7.3.3 Rat2 fibroblasts

Rat2 cells, similar to HeLa cells, were mainly restricted by the protein patterns in regard of migration and spreading. They barely migrated from the pattern onto the AF layer. Compared to the grid without AF layer, they spread only very slow, although the adherence to the carbon surface happened very fast, compared to the other cell types. More cells were observed on the grid with fully intact AF layer compared to HeLa or B16-F1 cells, although completely unable to spread or proliferate. The few proliferation events observed happened very late in the course of the 12 hours. Regarding the influence of the pattern shapes on the morphology, Rat2 cells spread on the patterns with bigger area available, namely the dumbbell and cross-patterns. On the circle and fan-shaped patterns, Rat2 cells were observed in most cases in their spherical form. If the seeded Rat2 cells are to fixed for downstream EM acquisition, 7 hours after cell seeding is a good timepoint to perform the fixation, as most cells are than in a spread state, but no cell duplication happened at this point.

7.4 Comparison of the developed protocol to other workflows for photo patterning of EM grids

The protocol presented here orientated on different factors impacting the quality of micropatterning the EM grids, and aimed to reduce the grid handling and hand-on time required to pattern the grids as much as possible, and to minimize the usage of materials and reagents.

Other protocols published in recent years were compared in regard of these factors, to evaluate the advantages and shortcomings of the proposed strategy (see Figure 28). All workflows used to compare the here described protocol use the 2-step strategy to graft the AF layer with PLL and PEG-SVA, as well as the PLPP gel photo initiator and the PRIMO 2 system for AF layer depletion. In the first step, the EM grids were rendered hydrophilic using either plasma cleaning machines [20], [24] or glow dischargers [39]. The functionality of both machines was evaluated in this work, the effect seems not to be influenced by the type of machine.

The effectivity of the AF layer depends on the concentration and incubation time of the grid in the PLL- and subsequently in the PEG-SVA solutions. The concentration of PLL used mostly was 0.01%, and the incubation either 1 hour at RT or overnight at 4 °C [20], [24], [39]. As evaluated in this work, 30 minutes incubation at RT of the PLL solution is sufficient to coat the grid surface, and is also recommended in the application note by Alvèole [61]. The PEG-SVA for grafting the PLL-PEG layer is used mostly in a 1-hour incubation at room temperature. This step is essential to give the grid it's AF capacity, and was changed only in one of the other protocols to half the concentration, but double the incubation time [20].

The protocols for photopatterning of EM grids used to compare this work to differ the most in the details for applying the photo initiator, as well as in the UV exposure used to digest the AF layer. The PLPP gel photo initiator was applied either pure [20], [24] or in different dilutions in EtOH [39], [61]. As evaluated in this work, the dilution of the gel in EtOH comes with the advantage, that air bubbles are removed from the gel. The biggest differences in the protocols were noted in regard of the UV exposures with the PRIMO systems. When projected directly on the PLL-PEG layer, the UV exposure ranges from 40 mJ/mm^2 [61] over 50 mJ/mm^2 [39] up to 800-1000 mJ/mm^2 [20]. In one recently published protocol, the UV was projected through a PDMS platform and through the carbon film on the AF layer, using 1200 mJ/mm^2. [24] According to the application note from Alvèole [61], the required UV exposure is about half when using the 365 nm LED light source compared to the 375 nm light originating from a laser source. Nevertheless, the exposure of 50 mJ/mm^2 used in the here described protocol was enough to digest the AF layer when projecting the UV light through the carbon layer (it should be noted that no PDMS platform had to be penetrated by the light additionally [24]). As the process of photo patterning can be pictured by light power (in mW) projected to receive a certain amount of energy transferred to a defined area (exposure, in mJ/mm^2), the only variable is the time of UV projection per field of view of the DMD. The higher the exposure is chosen, the longer the UV light of a certain power has to be projected to the same area and the longer the whole patterning process takes, per field of view of the DMD. If considered, that the PRIMO 2 system requires approximately half the UV dose compared to the PRIMO [61], the here proposed 50 mJ/mm^2 speed up the patterning process by a factor of 12. This comparison was done with the protocol published by Dow et al., where the light was projected through the carbon film and an exposure of 1200 mJ/mm^2 was used with the first version of the PRIMO device [24].

Regarding the functionalization of the EM grids with different adhesive molecules, it is harder to draw clear conclusions compared with other protocols, as different ECM proteins were used. Two factors are important to mention here: i) the concentration of the molecule in solution, ii) the time of incubation on the patterned EM grid. In general, for different ECM proteins like fibronectin or laminin, a concentration of 25-100 µg/ml is used for a 1-hour incubation [20], [24]. Other ECM proteins, like gelatin, are used in a 1 mg/ml concentration and incubated for 1 hour [39]. The protocol proposed by Alvèole [61] recommends for the ECM protein fibrinogen a concentration of 25-100 µg/ml and an incubation time of maximal 15 minutes, to reduce background signal as much as possible. These numbers are highly dependent on the cell type used in the end to be seeded on the EM grids.

The number of cells differs also greatly between different protocols, dependent on the type of cell line used for seeding. The difference between the protocol described in this work and the others is the use of EM grid holders, to reduce the number of cells required for seeding to a number of about 2000 cells/grid. The protocol from Toro-Nahuelpan et al. states a cell number of 20,000 cells seeded per cm^2 [20]. An EM grid with 3 mm diameter has a total area of 7.07 mm^2, or 0.0707 cm^2, resulting in a number of 1,414 HeLa cells/grid in case of HeLa cells, and 565 RPE1 cells per grid [20]. These numbers are relatively low compared to all other protocols used for comparison here, leading to the assumption that further fine tuning of the seeding procedure is possible to work with even smaller number of cells seeded per grid.

For washing non-attached cells off the EM grid, the incubation time is again strongly dependent on the cell type. The strategy is in general always the same, by flushing the grid with fresh cell culture medium. At this point, the here proposed protocol is in disadvantage compared to the other protocols, as the wash-off is difficult to perform when the grids are mounted in the grid holders and placed in a 96-well plate.

Paper	PLL	PEG-SVA	PLPP	UV Exposure (* PRIMO; ** PRIMO 2)	ECM protein	Cell Type	Cell Count	Incubation time
Schuster (2023)	0.01%, 30 min, RT	100 mg/ml, 1 h, RT	3 µl, 1:3 gel dilution	**50 mJ/mm² **(through carbon)**	Laminin 25-50 µg/ml, 1 h	HeLa B16-F1 Rat2	1.5x10⁵ cells/ml 2.000 cells/grid	2 h, wash-off; 1.5 h, wash-off; 30 min, wash off
Dow et al. (2022)	0.01%, o/n, RT	100 mg/ml, 1 h, RT	15 µl, pure gel	*1200 mJ/mm² **(through carbon)**	Fibronectin 50 µg/ml, 1 h	PTK-1 cells	50.000 cells/ml	2 h, rinse; 10 h, fix
Engel et al. (2022)	0.01%, o/n, 4 °C; or 1 h, RT	100 mg/ml, 1 h, RT	3 µl, 1:6 gel dilution	*50 mJ/mm²	Gelatin, 1 mg/ml, 1 h Matrigel, 1:400, 30 min Rhodamin 100 µg/ml, 1 h	HUVEC, HFF	n.a.	2 h, rinse; 30 min, rinse
Toro-Nahuelpan et al. (2020)	0.01%, o/n, RT	50 mg/ml, 1-2 h, RT	1-3 µl pure gel	*800-1000 mJ/mm²	Fibronectin 50 µg/ml, 1 h	HeLa RPE1	20.000 cells/cm² 8.000 cells/cm²	1.5-2 h; 20-35 min
Alvèole (2017)	0.01%, 30 min, RT	70-100 mg/ml, 1 h, RT	3 µl, 1:3 gel dilution	*40 mJ/mm²; **20mJ/mm²	Fibrinogen 20-100 µg/ml, 5-15 min	n.a.	n.a.	n.a.

Figure 28: Comparison of protocol for photo patterning of EM grids from different publications: The different factors evaluated in this work ("Schuster (2023)") compared to other published protocols. Listed are: the concentration and incubation time of the grid in Poly-L-Lysine (PLL) and PEG-SVA; the amount and, if performed, dilution of photo initiator (PLPP); the exposure to UV light projected by the PRIMO (*) or PRIMO 2 (**) system (UV exposure), "through carbon" indicates if the UV light was projected through the carbon film on the AF layer or directly on it by flipping the grid prior to UV exposure; the type of protein for functionalization and the respective incubation times (ECM protein); the cell type(s) used for the experiment (Cell Type); the number of cells seeded per grid, per area [cm^2] or in dilution (cells per ml or per grid); the incubation time of the cells before wash-off non-attached cells and, if applied, the additional time before fixation.

8 Acknowledgements

I want to thank my supervisor Gabriel Krens for the opportunity to finish my educational path with this thesis, and the whole team of the imaging facility for constant support and input. I want to thank Florian Schur for hosting me in his work group, and all the group members for sharing their expertise in their scientific field with me. I also want thank Barbara Hamilton and Angela Witte from the SPL for the constant support during my years on the University of Vienna. Further, I want to express my thanks to Irene Lichtscheidl, who sparked my interest in microscopy.

9 References

[1] L. Gan and G. J. Jensen, "Electron tomography of cells," *Quarterly Reviews of Biophysics*, vol. 45, no. 1. pp. 27–56, Feb. 2012. doi: 10.1017/S0033583511000102.

[2] R. F. Thompson, M. Walker, C. A. Siebert, S. P. Muench, and N. A. Ranson, "An introduction to sample preparation and imaging by cryo-electron microscopy for structural biology," *Methods*, vol. 100, pp. 3–15, May 2016, doi: 10.1016/j.ymeth.2016.02.017.

[3] Y. Tao, “A Historical Investigation of the Debates on the Invention and Invention Rights of Electron Microscope,” 2018.

[4] R. I. Koning and A. J. Koster, “Cryo-electron tomography in biology and medicine,” *Annals of Anatomy*, vol. 191, no. 5. pp. 427–445, 2009. doi: 10.1016/j.aanat.2009.04.003.

[5] F. K. Schur, “Toward high-resolution in situ structural biology with cryo-electron tomography and subtomogram averaging,” *Current Opinion in Structural Biology*, vol. 58. Elsevier Ltd, pp. 1–9, Oct. 01, 2019. doi: 10.1016/j.sbi.2019.03.018.

[6] J. Dubochet and A. W. McDowall, “VITRIFICATION OF PURE WATER FOR ELECTRON MICROSCOPY,” *J Microsc*, vol. 124, no. 3, pp. 3–4, 1981, doi: 10.1111/j.1365-2818.1981.tb02483.x.

[7] M. Adrian, J. Dubochet, J. Lepault, and A. W. McDowall, “Cryo-electron microscopy of viruses.”

[8] H. Moor, “Theory and Practice of High Pressure Freezing,” in *Cryotechniques in Biological Electron Microscopy*, Berlin, Heidelberg: Springer Berlin Heidelberg, 1987, pp. 175–191. doi: 10.1007/978-3-642-72815-0_8.

[9] S. Reipert, I. Fischer, and G. Wiche, “High-pressure freezing of epithelial cells on sapphire coverslips,” 2004. doi: 10.1111/j.1365-2818.2004.01260.x.

[10] D. J. De Rosier and A. Klug, “Reconstruction of Three Dimensional Structures from Electron Micrographs,” 1966.

[11] A. J. Koster *et al.*, “Perspectives of Molecular and Cellular Electron Tomography,” 1997.

[12] T. Ishikawa, “Electron Tomography,” in *Encyclopedia of Cell Biology*, Elsevier Inc., 2016, pp. 22–31. doi: 10.1016/B978-0-12-394447-4.20006-0.

[13] M. Krause and A. Gautreau, “Steering cell migration: Lamellipodium dynamics and the regulation of directional persistence,” *Nature Reviews Molecular Cell Biology*, vol. 15, no. 9. Nature Publishing Group, pp. 577–590, 2014. doi: 10.1038/nrm3861.

[14] P. K. Mattila and P. Lappalainen, “Filopodia: Molecular architecture and cellular functions,” *Nature Reviews Molecular Cell Biology*, vol. 9, no. 6. pp. 446–454, Jun. 10, 2008. doi: 10.1038/nrm2406.

[15] W. H. Escovitz, T. R. Fox, and R. Levi-Setti, “Scanning Transmission Ion Microscope with a Field Ion Source (ion optics/field ionization/microradiography),” 1975.

[16] M. Marko, C. Hsieh, W. Moberlychan, C. A. Mannella, and J. Frank, “Focused ion beam milling of vitreous water: Prospects for an alternative to cryo-ultramicrotomy of frozen-hydrated biological samples,” *J Microsc*, vol. 222, no. 1, pp. 42–47, Apr. 2006, doi: 10.1111/j.1365-2818.2006.01567.x.

[17] M. Marko, C. Hsieh, R. Schalek, J. Frank, and C. Mannella, “Focused-ion-beam thinning of frozen-hydrated biological specimens for cryo-electron microscopy,” *Nat Methods*, vol. 4, no. 3, pp. 215–217, Mar. 2007, doi: 10.1038/nmeth1014.

[18] A. Rigort *et al.*, “Micromachining tools and correlative approaches for cellular cryo-electron tomography,” *J Struct Biol*, vol. 172, no. 2, pp. 169–179, Nov. 2010, doi: 10.1016/j.jsb.2010.02.011.

[19] J. He *et al.*, “Cryo-FIB specimen preparation for use in a cartridge-type cryo-TEM,” *J Struct Biol*, vol. 199, no. 2, pp. 114–119, Aug. 2017, doi: 10.1016/j.jsb.2017.05.011.

[20] M. Toro-Nahuelpan, I. Zagoriy, F. Senger, L. Blanchoin, M. Théry, and J. Mahamid, “Tailoring cryo-electron microscopy grids by photo-micropatterning for in-cell structural studies,” *Nat Methods*, vol. 17, no. 1, pp. 50–54, Jan. 2020, doi: 10.1038/s41592-019-0630-5.

[21] S. L. K. Bowers, I. Banerjee, and T. A. Baudino, “The extracellular matrix: At the center of it all,” *Journal of Molecular and Cellular Cardiology*, vol. 48, no. 3. pp. 474–482, Mar. 2010. doi: 10.1016/j.yjmcc.2009.08.024.

[22] A. C. Erickson and J. R. Couchman, “Still More Complexity in Mammalian Basement Membranes,” 2000. [Online]. Available: http://www.jhc.org

[23] C. Van Der Putten *et al.*, “Protein Micropatterning in 2.5D: An Approach to Investigate Cellular Responses in Multi-Cue Environments,” *ACS Appl Mater Interfaces*, vol. 13, no. 22, pp. 25589–25598, Jun. 2021, doi: 10.1021/acsami.1c01984.

[24] L. P. Dow *et al.*, “Morphological control enables nanometer-scale dissection of cell-cell signaling complexes,” *Nat Commun*, vol. 13, no. 1, Dec. 2022, doi: 10.1038/s41467-022-35409-9.

[25] A. Bernard, E. Delamarche, H. Schmid, B. Michel, H. R. Bosshard, and H. Biebuyck, “Printing patterns of proteins,” *Langmuir*, vol. 14, no. 9, pp. 2225–2229, Jan. 1998, doi: 10.1021/la980037l.

[26] A. B. Braunschweig, F. Huo, and C. A. Mirkin, “Molecular printing,” *Nat Chem*, vol. 1, no. 5, pp. 353–358, Aug. 2009, doi: 10.1038/nchem.258.

[27] P. O. Strale, A. Azioune, G. Bugnicourt, Y. Lecomte, M. Chahid, and V. Studer, “Multiprotein Printing by Light-Induced Molecular Adsorption,” *Advanced Materials*, vol. 28, no. 10, pp. 2024–2029, Mar. 2016, doi: 10.1002/adma.201504154.

[28] A. Kumar and G. M. Whitesides, “Features of gold having micrometer to centimeter dimensions can be formed through a combination of stamping with an elastomeric stamp and an alkanethiol ‘“ink”’ followed by chemical etching,” *Appl Phys Lett*, vol. 63, no. 14, pp. 2002–2004, Oct. 1993, doi: 10.1063/1.110628.

[29] M. Théry, “Micropatterning as a tool to decipher cell morphogenesis and functions,” *Journal of Cell Science*, vol. 123, no. 24. pp. 4201–4213, Dec. 15, 2010. doi: 10.1242/jcs.075150.

[30] J. M. Bélisle, J. Mazzaferri, and S. Costantino, “Laser-assisted adsorption by photobleaching,” in *Methods in Cell Biology*, Academic Press Inc., 2014, pp. 125–140. doi: 10.1016/B978-0-12-416742-1.00007-X.

[31] A. Martinez-Rivas, G. K. González-Quijano, S. Proa-Coronado, C. Séverac, and E. Dague, “Methods of micropatterning and manipulation of cells for biomedical applications,” *Micromachines*, vol. 8, no. 12. MDPI AG, Nov. 29, 2017. doi: 10.3390/mi8120347.

[32] L. Engel *et al.*, “Extracellular matrix micropatterning technology for whole cell cryogenic electron microscopy studies,” *Journal of Micromechanics and Microengineering*, vol. 29, no. 11, Sep. 2019, doi: 10.1088/1361-6439/ab419a.

[33] T. Vignaud, H. Ennomani, and M. Théry, “Polyacrylamide Hydrogel Micropatterning,” in *Methods in Cell Biology*, Academic Press Inc., 2014, pp. 93–116. doi: 10.1016/B978-0-12-417136-7.00006-9.

[34] C. Stoecklin *et al.*, “A New Approach to Design Artificial 3D Microniches with Combined Chemical, Topographical, and Rheological Cues,” *Adv Biosyst*, vol. 2, no. 7, Jul. 2018, doi: 10.1002/adbi.201700237.

[35] B. S. Sibert, J. Y. Kim, J. E. Yang, and E. R. Wright, “Micropatterning transmission electron microscopy grids to direct cell positioning within whole-cell cryo-electron tomography workflows,” *Journal of Visualized Experiments*, vol. 2021, no. 175, Sep. 2021, doi: 10.3791/62992.

[36] “http://www.acdlabs.com/products/chem_dsn_lab/chemsketch/.”

[37] Q. Chen *et al.*, “Impact of Antifouling PEG Layer on the Performance of Functional Peptides in Regulating Cell Behaviors,” *J Am Chem Soc*, vol. 141, no. 42, pp. 16772–16780, Oct. 2019, doi: 10.1021/jacs.9b07105.

[38] C. Melero *et al.*, “Light-induced molecular adsorption of proteins using the primo system for micro-patterning to study cell responses to extracellular matrix proteins,” *Journal of Visualized Experiments*, vol. 2019, no. 152, Oct. 2019, doi: 10.3791/60092.

[39] L. Engel, R. Held, C. G. Vasquez, W. I. Weis, and A. R. Dunn, “Micropatterning EM grids for cryo-electron tomography of cells,” 2022, doi: 10.17504/protocols.io.bz22p8ge.

[40] C. J. Dalton and C. A. Lemmon, “Fibronectin: Molecular structure, fibrillar structure and mechanochemical signaling,” *Cells*, vol. 10, no. 9. MDPI, Sep. 01, 2021. doi: 10.3390/cells10092443.

[41] J. W. Weisel and R. I. Litvinov, “Fibrin formation, structure and properties,” *Subcell Biochem*, vol. 82, pp. 405–456, Jan. 2017, doi: 10.1007/978-3-319-49674-0_13.

[42] “http://www.BioRender.com/.”

[43] M. Aumailley and N. Smyth, “The role of laminins in basement membrane function,” 1998.

[44] B. Alberts *et al.*, *THE CELL Molecular Biology of Sixth Edition*, 6th ed. Garland Science, Taylor & Francis Group, LLC, 2008.

[45] D. J. Ncayiyana, “HeLa Ncayiyana. 2011. The extraordinary story of the life after death of Henrietta Lacks,” *SAMJ: South African Medical Journal*, vol. 101, no. 3, pp. 141–141, 2011.

[46] M. Boshartb93, L. Gissmann2, H. Ikenberg2, A. Kleinheinzl, W. Scheurlen2, and H. Zur Hausen2, “A new type of papillomavirus DNA, its presence in genital cancer biopsies and in cell lines derived from cervical cancer,” 1984.

[47] M. Scheffner, K. Munger, J. C. Byrne, and P. M. Howley, “The state of the p53 and retinoblastoma genes in human cervical carcinoma cell lines,” 1991.

[48] R. L. Holland, K. D. Bosi, A. Seeger, and S. R. Blanke, “Restoration of mitochondrial structure and function within Helicobacter pylori VacA intoxicated cells”, doi: 10.1101/2023.05.19.540400.

[49] K. Fairman and B. S. Jacobson, “UNIQUE MORPHOLOGY OF HeLa CELL ATTACHMENT, SPREADING AND DETACHMENT FROM MICROCARRIER BEADS COVALENTLY COATED WITH A SPECIFIC AND NON-SPECIFIC SUBSTRATUM.”

[50] J. M. Ubellacker *et al.*, “Lymph protects metastasizing melanoma cells from ferroptosis,” *Nature*, vol. 585, no. 7823, pp. 113–118, Sep. 2020, doi: 10.1038/s41586-020-2623-z.

[51] I. J. Fidler, “Biological behavior of malignant melanoma cells correlated to their survival in vivo.,” *Cancer Res*, vol. 35, no. 1, pp. 218–24, Jan. 1975.

[52] I. R. Nabi and A. Raz, “Loss of metastatic responsiveness to cell shape modulation in a newly characterized B16 melanoma adhesive cell variant,” 2014. [Online]. Available: http://cancerres.aacrjournals.org/content/48/5/1258#related-urls

[53] J. S. Kim *et al.*, “Characterization of morphological changes of B16 melanoma cells under natural killer cell attack,” *Int Immunopharmacol*, vol. 67, pp. 366–371, Feb. 2019, doi: 10.1016/j.intimp.2018.12.037.

[54] M. Ravikanth, P. Soujanya, K. Manjunath, T. R. Saraswathi, and C. R. Ramachandran, “Heterogenecity of fibroblasts,” *Journal of Oral and Maxillofacial Pathology*, vol. 15, no. 2, pp. 247–250, May 2011, doi: 10.4103/0973-029X.84516.

[55] W. C. Topp’, “Normal Rat Cell Lines Deficient in Nuclear Thymidine Kinase,” 1981.

[56] M. Peng, L. Huang, Z. Xie, W. H. Huang, and A. Askari, “Partial inhibition of Na+/K+-ATPase by ouabain induces the Ca2+-dependent expressions of early-response genes in cardiac myocytes,” *Journal of Biological Chemistry*, vol. 271, no. 17, pp. 10372–10378, Apr. 1996, doi: 10.1074/jbc.271.17.10372.

[57] K. Kawata *et al.*, “A Tumor Suppressor Gene Product, Platelet-Derived Growth Factor Receptor-Like Protein Controls Chondrocyte Proliferation and Differentiation,” *J Cell Biochem*, vol. 118, no. 11, pp. 4033–4044, Nov. 2017, doi: 10.1002/jcb.26059.

[58] F. Fäßler, G. Dimchev, V. V. Hodirnau, W. Wan, and F. K. M. Schur, “Cryo-electron tomography structure of Arp2/3 complex in cells reveals new insights into the branch junction,” *Nat Commun*, vol. 11, no. 1, Dec. 2020, doi: 10.1038/s41467-020-20286-x.

[59] F. Fäßler *et al.*, “ArpC5 isoforms regulate Arp2/3 complex-dependent protrusion through differential Ena/VASP positioning,” 2023.

[60] D. Murthy, K. S. Attri, and P. K. Singh, “Phosphoinositide 3-kinase signaling pathway in pancreatic ductal adenocarcinoma progression, pathogenesis, and therapeutics,” *Frontiers in Physiology*, vol. 9, no. APR. Frontiers Media S.A., Apr. 04, 2018. doi: 10.3389/fphys.2018.00335.

[61] Alvèole Lab, “PRIMO PROTOCOL: TEM grid photopatterning,” Jun. 2019. [Online]. Available: https://www.alveolelab.com/tutorials/micropatterning-tem-grid/

[62] M. Toro-Nahuelpan, I. Zagoriy, F. Senger, L. Blanchoin, M. Théry, and J. Mahamid, “Tailoring cryo-electron microscopy grids by photo-micropatterning for in-cell structural studies,” *Nat Methods*, vol. 17, no. 1, pp. 50–54, Jan. 2020, doi: 10.1038/s41592-019-0630-5.

[63] F. Fäßler, B. Zens, R. Hauschild, and F. K. M. Schur, “3D printed cell culture grid holders for improved cellular specimen preparation in cryo-electron microscopy,” *J Struct Biol*, vol. 212, no. 3, Dec. 2020, doi: 10.1016/j.jsb.2020.107633.

[64] Alvèole Lab, “DRAWING MICROPATTERNS FOR,” Feb. 2017.

[65] J. Schindelin *et al.*, “Fiji: An open-source platform for biological-image analysis,” *Nature Methods*, vol. 9, no. 7. pp. 676–682, Jul. 2012. doi: 10.1038/nmeth.2019.

[66] X. Liu, B. Peng, W. Zhang, J. Zhu, X. Liu, and M. Wei, “Improvement of high-temperature stability of Al2O3/Pt/ZnO/Al2O3 film electrode for SAW devices by using Al2O3 barrier layer,” *Materials*, vol. 10, no. 12, Dec. 2017, doi: 10.3390/ma10121377.

[67] P. Lakkala, S. R. Munnangi, S. Bandari, and M. Repka, “Additive manufacturing technologies with emphasis on stereolithography 3D printing in pharmaceutical and medical applications: A review,” *Int J Pharm X*, vol. 5, Dec. 2023, doi: 10.1016/j.ijpx.2023.100159.